

Contents

1	Introduction	1
1.1	Background To The Research Problem	1
1.2	Literature Review	2
1.3	Objectives	5
1.4	Organisation Of Thesis	6
2	Proposed System And Droop Control Strategy	7
2.1	Proposed System	7
2.1.1	Voltage Source Inverter	8
2.1.2	Filter	8
2.1.3	Internal Controller	9
2.1.4	Droop Control Strategy	10
2.2	Conventional Droop-Controls Used For GCDCDGs	10
2.3	Proposed Droop Control Strategy	12
3	Internal Controller Strategies	16
3.1	PI Based Internal Controller	16
3.1.1	Key Components of PI Controller	17
3.1.2	Benefits of PI Controller	17
3.2	ANN Based Internal Controller	19

3.2.1	Key Components of ANN Based Controller	19
3.2.2	Neural Network Architecture	20
3.2.3	Advantages Of ANN Over PI Based Controller	21
3.2.4	Design Of ANN Based Internal Control Strategy	22
3.3	MPC Based Internal Controller	24
3.3.1	Advantages of MPC	25
3.3.2	Disdvantages of MPC	25
3.3.3	Design of MPC	26
3.3.4	State-Space Representation Of The Proposed System	26
3.3.5	Cost Function	28
3.3.6	MPC Main Program	28
4	Simulation, Results and Discussions	30
4.1	Implementation Of The Proposed Droop Control Strategy	30
4.1.1	Case 1: UG Frequency Drop Without Proposed Strategy	33
4.1.2	Case 2: UG Frequency Drop With Proposed Strategy	34
4.1.3	Case 3: UG Voltage Magnitude Drop Without Proposed Strat- egy	36
4.1.4	Case 4: UG Voltage Magnitude Drop With Proposed Strategy	37
4.1.5	Case 5: UG Frequency And Voltage Magnitude Drop With Balanced Load Injection	39
4.1.6	Case 6: UG Frequency And Voltage Magnitude Drop With Induction Motor Load Switching	41
4.2	Implementation Of ANN Based Controller	44
4.2.1	Case 1: UG Frequency Drop	44
4.2.2	Case 2: UG Voltage Magnitude	48

4.2.3	Case 3: UG Frequency And Voltage Magnitude Drop With Balanced Load Injection	51
4.2.4	Case 4: UG Frequency And Voltage Magnitude Drop With Induction Motor Load Switching	55
4.3	Implementation and Comparison With MPC Based Controller	59
4.3.1	Case 1: UG Frequency Drop	60
4.3.2	Case 2: UG Voltage Magnitude Drop	62
4.3.3	Case 3: UG Frequency And Voltage Magnitude Drop With Balanced Load Injection	63
5	Conclusion	66
5.1	Future Scope	67
	Bibliography	71

List of Figures

2.1	Main Block Diagram	7
2.2	Internal Controller Block Diagram	9
2.3	P- ω droop characteristics	12
2.4	P- ω and Q- V droop characteristics	14
2.5	P and I _d limiter	15
2.6	Q and I _q limiter	15
3.1	Simple Illustration of a PI Controller	17
3.2	Typical Neural Network Architecture	20
3.3	ANN based Internal Controller Strategy	23
3.4	Proposed System With MPC	27
3.5	MPC Main Algorithm	29
4.1	Main Simulation Diagram	31
4.2	GCDGDG Controller Without Proposed Strategy	32
4.3	GCDGDG Controller With Proposed Strategy	33
4.4	DG, Grid Frequency vs Time	33
4.5	Output d _q Currents vs Time	34
4.6	Output Active and Reactive Power vs Time	34
4.7	DG, Grid Frequency vs Time	35

4.8	Output dq Currents vs Time	35
4.9	Output Active And Reactive Power vs Time	35
4.10	Output abc Currents vs Time	35
4.11	DG, Grid Voltage vs Time	36
4.12	Output dq Currents vs Time	37
4.13	Output Active and Reactive Power vs Time	37
4.14	DG, Grid Voltage vs Time	37
4.15	Output dq Currents vs Time	38
4.16	Output Active and Reactive Power vs Time	38
4.17	Output abc Currents vs Time	38
4.18	DG, Grid Frequency vs Time	39
4.19	DG, Grid Voltage vs Time	39
4.20	Output dq Currents vs Time	40
4.21	Output Active and Reactive Power vs Time	40
4.22	Active and Reactive Components of Balanced Load vs Time	40
4.23	Output abc Currents vs Time	40
4.24	DG, Grid Frequency vs Time	42
4.25	DG, Grid Voltage vs Time	42
4.26	Output dq Currents vs Time	42
4.27	Output Active and Reactive Power vs Time	42
4.28	Active and Reactive Components of Induction Motor Load vs Time .	43
4.29	Output abc Currents vs Time	43
4.30	GCDCDG Controller With Proposed Strategy and ANN	44
4.31	DG, Grid Frequency vs Time	45
4.32	Output dq Currents vs Time(PI)	45
4.33	Output dq Currents vs Time(ANN)	45
4.34	Output Active and Reactive Power vs Time (PI)	45

4.35 Output Active and Reactive Power vs Time (ANN)	46
4.36 Output abc Currents vs Time(PI)	46
4.37 Output abc Currents vs Time(ANN)	46
4.38 PI Based GCDCDG	47
4.39 ANN Based GCDCDG	47
4.40 DG, Grid Voltage vs Time	48
4.41 Output dq Currents vs Time (PI)	48
4.42 Output dq Currents vs Time (ANN)	48
4.43 Output Active and Reactive Power vs Time(PI)	49
4.44 Output Active and Reactive Power vs Time(ANN)	49
4.45 Output abc Current VS Time(PI)	49
4.46 Output abc Current VS Time(ANN)	49
4.47 PI Based GCDCDG	50
4.48 ANN Based GCDCDG	50
4.49 DG, Grid Frequency vs Time	51
4.50 DG, Grid Voltage vs Time	52
4.51 Output dq Currents vs Time(PI)	52
4.52 Output dq Currents vs Time(ANN)	52
4.53 Output Active and Reactive Power vs Time(PI)	52
4.54 Output Active and Reactive Power vs Time(ANN)	53
4.55 Active and Reactive Components of Balanced Load vs Time	53
4.56 Output abc Currents vs Time (PI)	53
4.57 Output abc Currents vs Time (ANN)	53
4.58 PI Based GCDCDG	54
4.59 ANN Based GCDCDG	54
4.60 DG, Grid Frequency vs Time	55
4.61 DG, Grid Voltage vs Time	56

4.62 Output dq Currents vs Time(PI)	56
4.63 Output dq Currents vs Time(ANN)	56
4.64 Output Active and Reactive Power vs Time(PI)	56
4.65 Output Active and Reactive Power vs Time(ANN)	57
4.66 Active and Reactive Components of Induction Motor Load vs Time . .	57
4.67 Output abc Currents vs Time (PI)	57
4.68 Output abc Currents vs Time (ANN)	58
4.69 PI Based GCDCDG	58
4.70 ANN Based GCDCDG	59
4.71 MPC Block diagram	60
4.72 DG, Grid Frequency vs Time	60
4.73 Output abc Currents vs Time	61
4.74 Output Current THD at Steady State with MPC Controller	61
4.75 DG, Grid Voltage vs Time	62
4.76 Output abc Currents vs Time	62
4.77 Output Current THD at Steady State with MPC Controller	62
4.78 DG, Grid Frequency vs Time	63
4.79 DG, Grid Voltage vs Time	63
4.80 Output abc Currents vs Time	64
4.81 Active and Reactive Components of Balanced Load vs Time	64
4.82 Output Current THD at Steady State with MPC Controller	64

1 Introduction

1.1 Background To The Research Problem

Grid-connected distributed generation (DGs) are widely employed to meet consumer energy needs. These small-scale power plants typically connected to the grid through power inverters. The inverter-interfaced DGs are equipped with a droop control mechanism to supply the necessary power to the connected power system. Droop control is a common technique used to improve the stability of power systems that rely heavily on grid-connected inverters, and it achieves this without requiring communication between individual units.

There are two primary concerns regarding Grid Connected Droop Controlled Distributed Generators (GCDCDGs). The first, which has been extensively studied, is the stability of the droop control strategy. The second involves keeping the current below a specified maximum limit. It's crucial for a GCDCDG to have a current-limiting feature that remains active under both normal and abnormal grid conditions. This project introduces a novel droop-control-based strategy to achieve current limitation in GCDCDGs without resorting to external current limiters, thus ensuring stable operation under different conditions.

The proportional-integral (PI) controller is a commonly used method for controlling voltage source converters (VSCs) and has proven successful in traditional power

systems primarily composed of synchronous generators. However, the growing integration of VSC-based renewable energy sources (RESs) has presented new challenges, and the same steady-state and transient performance may not be achievable with the conventional PI controller.

Model predictive controllers (MPCs), in contrast, have shown considerable success in effectively managing VSCs during dynamic and disturbance events. In a typical MPC implementation, the controller utilizes measurements of the system's current state and a dynamic model to forecast its behavior over a set period. It then determines an optimal control sequence that minimizes a cost function while adhering to constraints on the system's inputs, outputs, and states. This optimal control sequence is applied, and the process repeats at subsequent time steps. However, despite its numerous advantages, the primary drawbacks of MPC, such as high computational demands and increased time consumption, make it less appealing, particularly in smaller-scale applications like solar and wind energy systems, consumer electronics, and low-power embedded systems.

This challenge has encouraged researchers to seek a middle ground that can maintain the benefits of nonlinear controllers like MPC while reducing computational demands. One promising avenue is to utilize computationally efficient artificial intelligence (AI) techniques to replicate the performance of MPC or other advanced nonlinear controllers.

1.2 Literature Review

Inverter-based distributed generators (DGs) are commonly equipped with droop control mechanisms to help maintain power system stability. This allows them to contribute to the overall power supply of the grid. Droop control is particularly beneficial in situations where communication between different inverter units is limited or un-

available [1]-[4]. A current-limiting droop controller should have the capability to be operated in the set mode to accurately send the desired power to the grid or in the droop mode to take part in the grid regulation, while maintaining the inverter current below a given value at all times [5].

Two main considerations arise concerning grid-connected distributed generators (GCDCDGs). The first involves the stability of droop control strategies, a topic that has been extensively researched [6]-[8]. The second pertains to ensuring that current levels remain below a specified maximum threshold [9]-[14]. Current-limiting controllers can effectively restrict current levels by activating specifically designed protection circuits[16] or employing various Low-Voltage Ride Through (LVRT) structures [17],[18]. However, these methods pose challenges in proving their stability. External limiters and saturation units are frequently incorporated into current or voltage control loops to constrain output current. However, these additions can sometimes introduce unwanted oscillations and instability [9].

A recent development in current-limiting droop controllers [5], designed for single-phase grid-connected inverters, allows operation in both normal and faulty grid conditions. Unlike traditional methods, this controller achieves current limitation without the need for external limiters while ensuring system stability. In a study on photovoltaic (PV) grid-forming inverters [20], researchers explored a modified droop control to enable operation during abnormal grid voltage conditions. This proposed approach incorporated current-limiting control with Low-Voltage Ride Through (LVRT) capabilities. In reference [21], a unified current-limiting control scheme for grid-connected inverters is proposed. This scheme addresses both normal and faulty grid conditions while incorporating a simplified voltage support mechanism. The paper specifically examines current limiting in grid-connected distributed generators (GCDCDGs) within grid-connected microgrids (GCMGs) when facing under-grid (UG) frequency and/or voltage magnitude drops. This paper [22] introduces a novel droop-control-

based strategy to limit the output currents of grid-connected distributed generators (GCDCDGs). Notably, this approach eliminates the need for current limiters, ensuring stable operation even in challenging conditions like UG frequency and/or voltage magnitudes, balanced load injections, induction motor load injection etc.

The vector proportional integral (PI) controller, a prevalent control technique for voltage source converters (VSCs), has proven successful in conventional power systems primarily composed of synchronous generators [23],[24]. However, the growing integration of renewable energy sources (RESs) based on VSCs has presented new challenges. The traditional PI controller may not guarantee consistent performance in both steady-state and transient conditions due to its limitations [25],[26]. These limitations include restricted control bandwidth, complexities in gain tuning, sensitivity to varying operating points, weak disturbance rejection, and reliance on accurate system parameter information.

Model predictive controllers (MPCs) have emerged as a promising solution for controlling voltage source converters (VSCs) under dynamic and varying conditions[27]. By predicting system behavior and optimizing control sequences, MPCs offer superior transient response, precise control, and the ability to handle system constraints[28],[29]. However, the computational demands and processing time required for MPCs make them less appealing for smaller-scale applications, such as solar and wind energy systems, consumer electronics, and low-power embedded systems. This has forced engineers to find some other strategies which offers lesser computational burden than MPC, while having better performance than PI controllers.

Artificial neural networks (ANNs), a subset of artificial intelligence, are widely employed in the power electronics and control field to accomplish a variety of goals[30],[31]. Additionally, ANNs have been applied in the field of control systems to optimize the gain tuning and weight factor design of PI and MPC controllers[32],[33],[34],[35]. Despite its applications, ANN-based control is often regarded as a "black box" approach

due to its lack of transparency in decision-making and unpredictable behavior in unfamiliar situations. This has led to a growing emphasis on performing stability and sensitivity analyses of ANN-controlled systems, particularly in industrial settings. A recent research focus has been on establishing specific boundary conditions during data generation and training processes to ensure the stability of ANN controllers [34],[35],[36].

1.3 Objectives

1. The first objective of this project is to develop a new control strategy based on the droop-control method, which has the following features:
 - To limit output power and current flow during Upstream Grid frequency drop.
 - To limit output power and current flow during Upstream Grid voltage magnitude drop.
 - To limit output power and current flow during Upstream Grid frequency and voltage magnitude drops and balanced load switching.
 - To limit output power and current flow during Upstream Grid frequency and voltage magnitude drops and unbalanced load switching.
2. The second objective of this project is to built upon the existing work by replacing the PI controllers in the internal controller with PI based ANN controllers to meet the following requirements (while also meeting power and current limiting demands in different cases as mentioned before):
 - To reduce the Total Harmonic Distortion (THD) of the output current supplied by GCDCDG to the grid in steady state.

-
- To reduce noise in power and current supplied by GCDCDG to the grid.
 - To improve time domain characteristics like rise time, fall time during disturbances like grid frequency or voltage variations, load switching etc.
3. The third objective of this project is to develop and compare the performance of MPC based controller with the PI based ANN controller. This is done to establish the viability of PI based ANN controller. Comparisons are made on the basis of following parameters :
- Total Harmonic Distortion (THD) of the output current supplied by GCD-CDG to the grid in steady state.

1.4 Organisation Of Thesis

This thesis work is divided into 5 chapters,

- Chapter 1 is the introduction chapter which summarises the project work, provides background information, provides literature review and clearly states objectives.
- Chapter 2 summarises proposed system and droop control strategy.
- Chapter 3 summarises different internal controllers used in the project work.
- Chapter 4 summarises simulink implementation and consists of results and discussions of different case studies.
- Chapter 5 consists of conclusion and future scope.

2 Proposed System And Droop Control Strategy

2.1 Proposed System

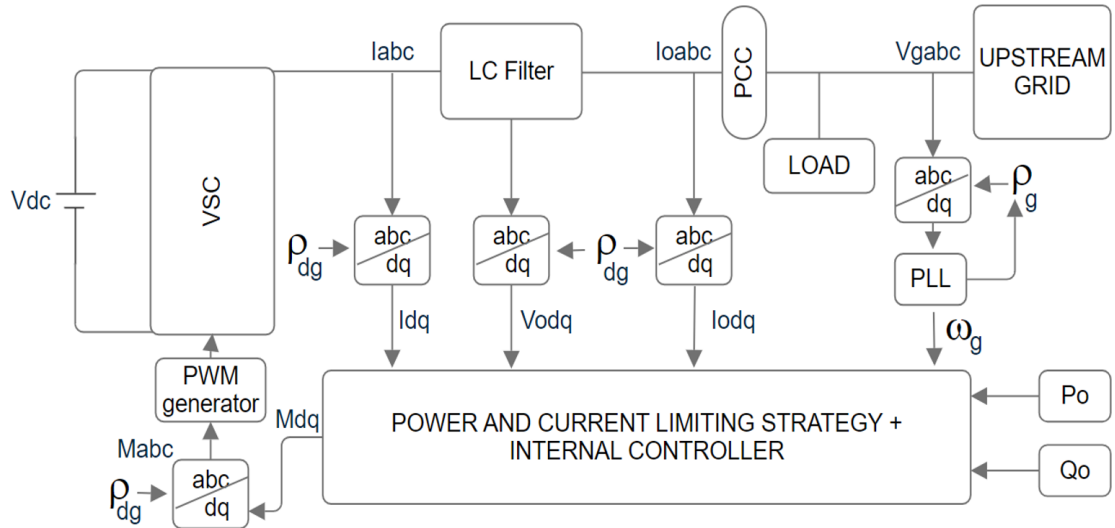


Figure 2.1: Main Block Diagram

The block diagram of the proposed system is shown in fig 2.1. The distributed generation is represented by a DC source V_{dc} . The voltage source inverter converts DC source into AC. The LC filter smoothes the inverter output, which is then fed to the upstream grid through a point of common coupling (PCC). The load is connected

to the PCC as well. Power and current limiting strategy and internal controller block inputs voltage and current measurements from inverter output, LC filter and PCC. P_0 and Q_0 represents the reference active and reactive power. ω_g represents the grid frequency, while ρ_g and ρ_{dg} represents grid and distributed generation angular frequency respectively.

The proposed system has the following components:

- Voltage Source Inverter
- Filter
- Internal Controller
- Droop Controlling Strategy

2.1.1 Voltage Source Inverter

The three-phase full-bridge inverter topology is used in this project. It is the simplest and most widely used structure for systems connected to the grid. It consists of six switches (IGBT), which are distributed as three bridges having two switches each. In order to generate a three-phase AC waveform, the three sets of bridges operate with 120° phase shift between them and can be represented by six states. Since each state has its own voltage and current values, it is also called a six-pulse (6P) inverter.

2.1.2 Filter

The output filter reduces the harmonics in generated current caused by semiconductor switching. There are several types of filters. The simplest variant is filter inductor connected to the inverter's output. Inductors are also used in combination with capacitors to get filters having LC or LCL configurations.

The first type is the L filter, it is a first order filter with attenuation 20 dB/decade over the whole frequency range. The second type is the LC filter, it is a second order filter and it has better damping behavior than L filter. This simple configuration is easy to design. The second order filter provides 12 dB/octave of attenuation after the cut-off frequency. The third type is the LCL filter. The attenuation of the LCL filter is 60 dB/decade for frequencies above resonant frequency, therefore lower switching frequency for the converter can be used. The LCL filter has good current ripple attenuation even with small inductance values. However it can bring also resonances and unstable states into the system. Therefore, the filter must be designed precisely according to the parameters of the specific converter.

LC filter is chosen over L and LCL filters, because of its relative simplicity and sufficient damping capabilities.

2.1.3 Internal Controller

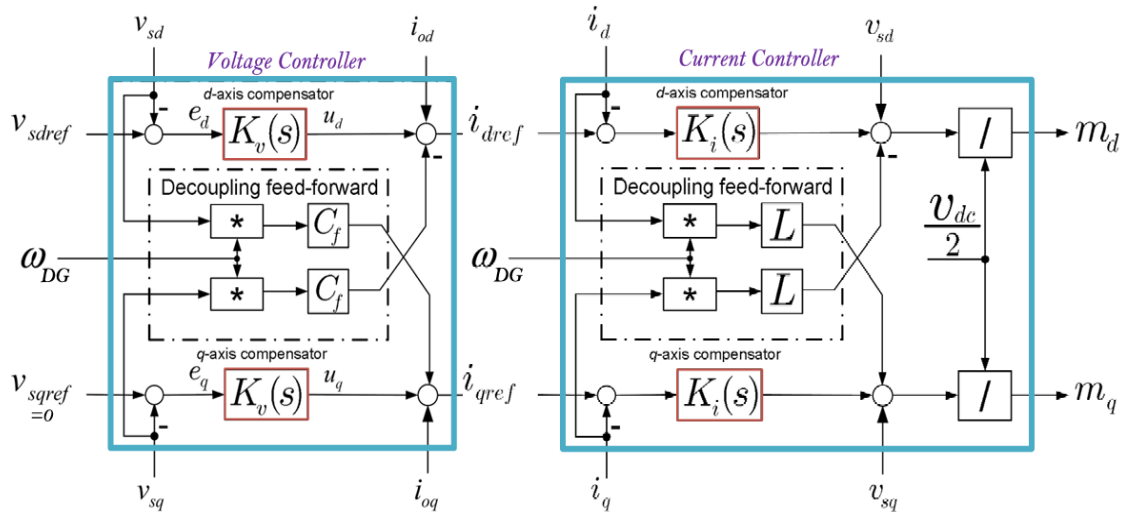


Figure 2.2: Internal Controller Block Diagram

Internal Controller consists of two loops. The outer loop is the voltage controller which produces reference currents i_{dref} and i_{qref} for the inner loop, which is called

the current loop. Current loop generates the switching signals (m_d , m_q). Pair of PI controllers are used in each loops. This is because here the internal controller operates in dq frame and both d and q components of voltage and current are decoupled. v_{sdref} and v_{sqref} are reference voltage values produced by the droop control strategy. v_{sd} and v_{sq} represents voltage measurement across the the filter capacitor. i_d , i_q , i_{od} and i_{oq} are d and q components of inverter output current and current measured at PCC respectively. ω_{dg} represents the angular frequency of the distributed generation.

2.1.4 Droop Control Strategy

Droop control Strategy will be explored in detail in the following sections.

2.2 Conventional Droop-Controls Used For GCD-CDGs

Reference of the DG frequency is determined as

$$\omega_{ref} = \omega_0 - m_p(P - P_0) \quad (2.1)$$

Where P is produced by low-pass filtering of $p = \frac{3}{2}(v_{od}i_{od})$ according to

$$P = \frac{\omega_c}{s + \omega_c} p \quad (2.2)$$

Where p represents instantaneous output active power of distributed generation, ω_0 represents rated frequency, m_p represents active power droop coefficient, ω_c represents cut off frequency.

Based on (2.1) when the DG injects rated active power at UG normal conditions the reference of the DG frequency is ω_0 . But under abnormal conditions when the UG frequency decreases, because of any reasons (for example suddenly increasing

demanded active power or decreasing power plant productions at UG), output active power of GCDCDG begins to increase and based on droop characteristic DG frequency decreases.

Reference of the DG voltage magnitude is determined as follows

$$V_{ref} = V_0 - n_q(Q - Q_0) \quad (2.3)$$

Where Q is produced by low-pass filtering of $q = -\frac{3}{2}(v_{od}i_{oq})$ according to

$$Q = \frac{\omega_c}{s + \omega_c} q \quad (2.4)$$

Where q is instantaneous output reactive power of the distributed generation, V_0 represents rated voltage, n_q represents reactive power droop coefficient.

Based on (2.3) when the DG injects rated reactive power at the UG normal conditions the reference of the DG voltage magnitude is PCC Voltage. But under the abnormal conditions when the UG voltage magnitude decreases, because of any reasons (for example short circuit faults at UG), output reactive power of GCDCDG begins to increase, and based on droop characteristic DG voltage magnitude decreases.

Under the above UG conditions, if UG frequency and/or voltage magnitude drops are large values, output powers of the GCDCDG may exceed their respective maximum values. One solution to limit the output powers to maximum values is by using current limiters to limit i_{od} and i_{od} to maximum values. This method in order to limit output reactive power performs correctly, but in output active power limiting a problem occurs. If UG frequency decreases, i_{od} increases, and if this increasing exceeds the maximum of i_{od} , the current limiter is saturated and according to P- ω droop characteristic the GCDCDG frequency does not track the UG frequency and this frequency difference, leads to power oscillation between DG and UG and the system becomes unstable. Also, increasing m_p to limit the output active power due

to stability limit is not possible. To overcome the aforementioned problems the proposed unified droop-control based current limiting strategy will be described in the next section.

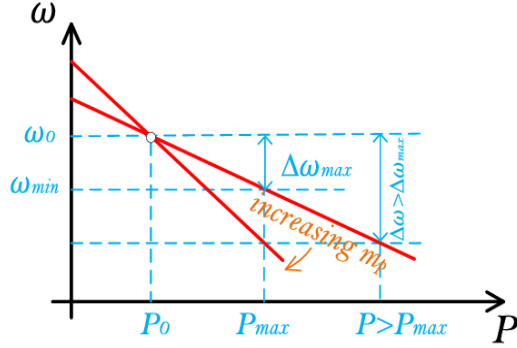


Figure 2.3: P- ω droop characteristics

2.3 Proposed Droop Control Strategy

In the proposed strategy, same as the conventional method the drop of DG frequency and voltage magnitude is based on increase in P and Q respectively. Thus (2.1) and (2.3) are used as previously used. According to (2.1) and (2.3), in steady-state, minimum values of ω_{ref} and V_{ref} occur at the maximum value of P and Q, respectively.

$$\omega_{min} = \omega_0 - m_p(P_{max} - P_0) \quad (2.5)$$

$$V_{min} = V_0 - n_q(Q_{max} - Q_0) \quad (2.6)$$

Thus, using (2.5) and (2.6), a maximum drop from rated values of frequency and voltage magnitude that protection strategy is not active are

$$\Delta\omega_{max} = \omega_{min} - \omega_0 = m_p(P_{max} - P_0) \quad (2.7)$$

$$\Delta V_{max} = V_{min} - V_0 = n_q(Q_{max} - Q_0) \quad (2.8)$$

According to P - ω and Q - V droop characteristics in Fig. 2.4 and Fig. 2.4 if frequency and voltage magnitude drops be greater than $\Delta\omega_{max}$ and ΔV_{max} , P and Q will be exceed the maximum values in steady-state, respectively. In the proposed method instead of increasing the droop coefficients to limit P and Q at their constraints, the droop curves move down after exceeding $\Delta\omega_{max}$ and ΔV_{max} , using two supplementary control signals as follows:

$$\omega_{ref} = \omega_0 - m_p(P - P_0 - \Delta P) \quad (2.9)$$

$$V_{ref} = V_0 - n_q(Q - Q_0 - \Delta Q) \quad (2.10)$$

where ΔP and ΔV are calculated so that P and Q limit to P_{max} and Q_{max} even after increasing of $\Delta\omega$ and ΔV from their maximums, respectively. Thus:

$$\Delta\omega = m_p(P_{max} - P_0 - \Delta P) \quad (2.11)$$

$$\Delta V = n_q(Q_{max} - Q_0 - \Delta V) \quad (2.12)$$

Note that (2.11) and (2.12) can be rewritten as

$$\begin{aligned} \Delta P &= \frac{-1}{m_p} \Delta\omega + (P_{max} - P_0), \quad \Delta\omega > \Delta\omega_{max} \\ &= 0, \quad \Delta\omega \leq \Delta\omega_{max} \end{aligned} \quad (2.13)$$

$$\begin{aligned} \Delta Q &= \frac{-1}{n_q} \Delta V + (Q_{max} - Q_0), \quad \Delta V > \Delta V_{max} \\ &= 0, \quad \Delta V \leq \Delta V_{max} \end{aligned} \quad (2.14)$$

where (2.13) and (2.14) limit P and Q to maximum values. Also, to ensure that in a transient state, instantaneous active and reactive power (i.e. p and q) and currents i_{od} and i_{oq} do not exceed their boundary values, two other supplementary control signals are added to (2.11) and (2.12), as

$$\omega_{ref} = \omega_0 - m_p(P - P_0 - \Delta P) + \delta\omega \quad (2.15)$$

$$V_{ref} = V_0 - n_q(Q - Q_0 - \Delta Q) + \delta V \quad (2.16)$$

where $\delta\omega$ and δV are respectively produced based on minimizing the difference between instantaneous and steady state values of i_{od} and i_{oq} by PI controllers. These supplementary control signals are

$$\begin{aligned}\delta\omega(s) &= \underbrace{\left(K_{P-id} + \frac{K_{I-id}}{S}\right)}_{G_p(s)} (I_{od} - i_{od}(s)) \\ \delta v(s) &= \underbrace{\left(K_{P-iq} + \frac{K_{I-iq}}{S}\right)}_{G_q(s)} (I_{oq} - i_{oq}(s))\end{aligned}$$

where,

$$I_{od} = \frac{\omega_c}{s + \omega_c} i_{od} \quad (2.17)$$

$$I_{oq} = \frac{\omega_c}{s + \omega_c} i_{oq} \quad (2.18)$$

Since steady-state values of currents are produced by low pass filtering instantaneous value of them and have not predefined values, to ensure that i_{od} and i_{oq} do not exceed their boundary values, I_{od} and I_{oq} signals are saturated at them. In the proposed scheme the steady-state power control is based on droop control, thus the current saturation mechanism does not deal with system instability.

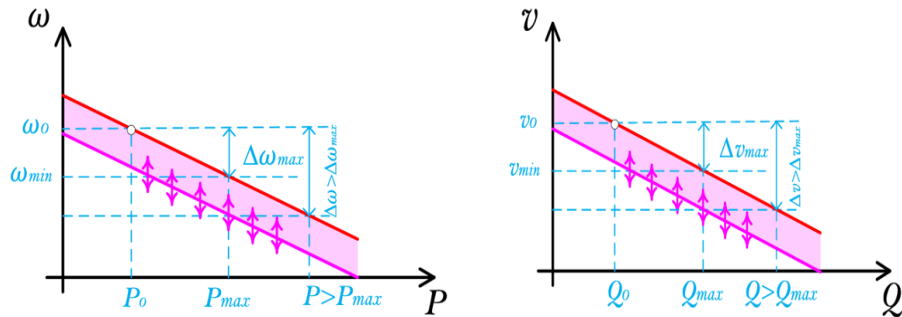


Figure 2.4: P- ω and Q- V droop characteristics

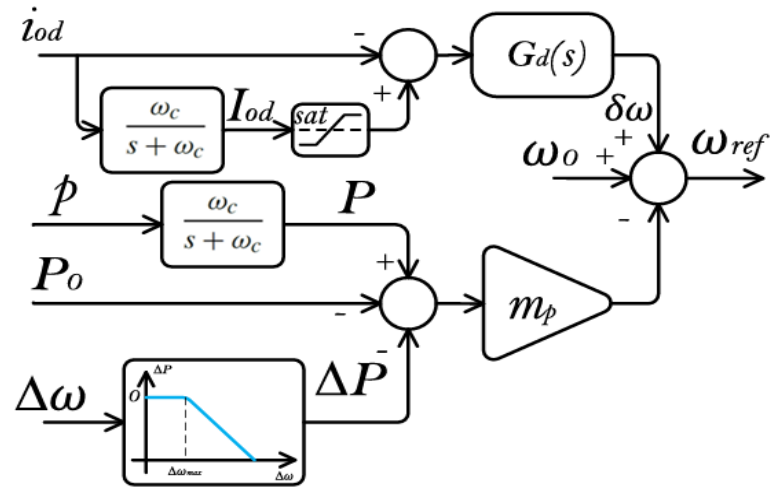


Figure 2.5: P and Iod limiter

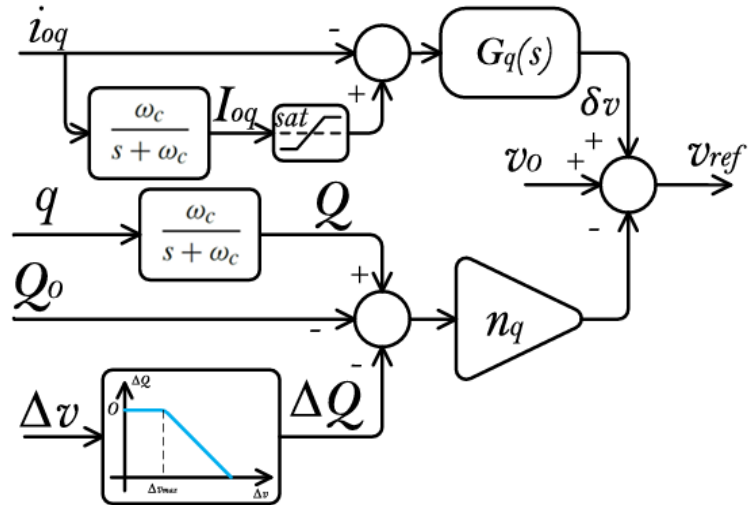


Figure 2.6: Q and Ioq limiter

Fig. 2.6 and Fig. 2.7 shows a block diagrams of the proposed droop-control based power and current limiting strategy. Both the block diagrams are derived from equations (2.15) and (2.16).

3 Internal Controller Strategies

This chapter covers the three different internal controller strategies used in this project work. Those three are :

1. PI Based Internal Controller
2. ANN Based Internal Controller
3. MPC Based Internal Controller

3.1 PI Based Internal Controller

A PI controller, or Proportional-Integral controller, is a type of feedback control mechanism widely used in industrial control systems and various other applications requiring continuous and precise control. It combines the actions of both proportional and integral control to adjust a process variable based on the error between the desired setpoint and the measured process variable. Block diagram of PI based internal controller was shown in the last chapter (Fig 2.2). Both voltage and current controller loops use a pair of PI controllers each. Fig 3.1 shows a simple illustration of a PI controller.

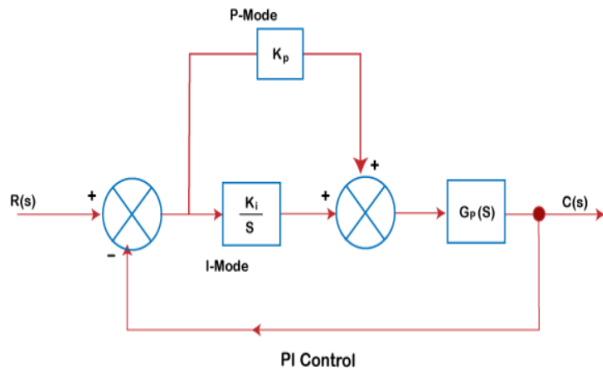


Figure 3.1: Simple Illustration of a PI Controller

3.1.1 Key Components of PI Controller

- **Proportional Control (P):** The proportional term generates a control signal that is directly proportional to the current error. A larger error leads to a larger corrective action, making the response faster. However, it may not eliminate steady-state errors completely.
- **Integral Control (I):** The integral term accumulates the past errors over time. It helps to eliminate steady-state errors by continually adjusting the control signal until the error is zero. This ensures that the process variable reaches and maintains the desired setpoint accurately.

3.1.2 Benefits of PI Controller

- **Elimination of Steady-State Error:** The integral term in a PI controller is specifically designed to address and eliminate steady-state errors. In the context of grid-connected inverters, this ensures that the inverter's output voltage and current precisely match the grid's voltage and frequency, even in the presence of disturbances or variations in the grid.
- **Fast Dynamic Response:** The proportional term in the PI controller pro-

vides a rapid response to sudden changes in the system. This is particularly beneficial in grid-connected inverters where fast response times are essential for maintaining grid stability and responding to fluctuations in power demand or generation.

- **Robustness to Parameter Variations:** PI controllers are generally less sensitive to variations in system parameters compared to other controllers. This makes them more robust in real-world applications where parameters can change due to environmental factors or aging of components.
- **Easy Implementation and Tuning:** PI controllers are relatively simple to implement in software or hardware and have only two parameters (proportional gain and integral gain) that need to be tuned. This simplicity makes them a cost-effective and widely adopted solution for grid-connected inverter control.
- **Zero Steady-State Error for Constant References/Disturbances:** The integral action ensures that the inverter output tracks constant reference signals (like desired power output) or rejects constant disturbances (like grid voltage variations) with zero steady-state error. This is crucial for maintaining accurate power control and ensuring grid compliance.

In spite of all these advantages PI controllers have the following limitations such as operation with limited control bandwidth, difficulty in gain tuning, more sensitivity toward different operating points, poor disturbance rejection capability, and the need for accurate system parameter information. The next controller strategy that we are going to discuss improves upon the following limitations.

3.2 ANN Based Internal Controller

Neural networks (also known as artificial neural networks or neural nets, abbreviated ANN or NN) are a branch of machine learning models inspired by the neuronal organization found in the biological neural networks in animal brains. An ANN is made of connected units or nodes called artificial neurons, which loosely model the neurons in a brain.

3.2.1 Key Components of ANN Based Controller

1. Artificial Neurons:

- These are the fundamental processing units of an ANN.
- They receive input from other neurons, perform a simple calculation, and then output a signal.
- Similar to biological neurons, artificial neurons have weighted connections. These weights determine the influence of each input on the output.

2. Activation Functions:

- Not all input signals are created equal. Activation functions introduce non-linearity into the network, allowing it to learn complex patterns.
- These functions take the weighted sum of the inputs and transform it into an output value. Common activation functions include sigmoid, ReLU (Rectified Linear Unit), and tanh.

3. Layers:

- Neurons are organized into layers. The first layer receives the raw input data. Subsequent layers, often called hidden layers, process the infor-

mation from the previous layer. The final layer generates the network's output.

- There can be one or more hidden layers, depending on the complexity of the problem the ANN is trying to solve.

3.2.2 Neural Network Architecture

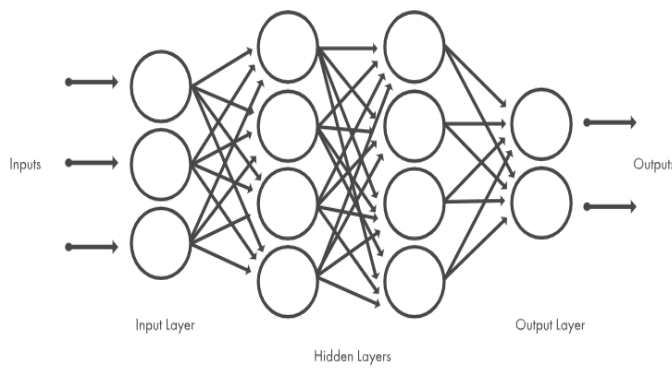


Figure 3.2: Typical Neural Network Architecture

There are three main types of layers in an Artificial Neural Network (ANN):

1. Input Layer:

This is the first layer of the network and acts as the entry point for data. The number of neurons in the input layer corresponds to the number of features in your input data. For example, if you're feeding an image into the network, the number of neurons might be equal to the number of pixels in the image. The input layer simply distributes the data to the next layer without any modification.

2. Hidden Layers:

These are the workhorses of the ANN and are responsible for extracting complex patterns from the data. There can be one or more hidden layers, and the

number of neurons in each layer significantly impacts the network's capabilities. Information from the previous layer is fed into the neurons of the hidden layer. Each neuron performs a weighted sum of these inputs and applies an activation function to generate an output. Hidden layers allow the network to learn intricate relationships between the input features and the desired output.

3. Output Layer:

This is the final layer of the network and provides the final prediction or classification. The number of neurons in the output layer depends on the problem you're trying to solve. For example, it might have one neuron for binary classification (yes/no) or multiple neurons for multi-class classification (identifying different types of objects). The output layer takes the processed information from the last hidden layer and generates the final result based on the chosen activation function.

3.2.3 Advantages Of ANN Over PI Based Controller

- **Handling Non-linearities:** PI controllers struggle with systems that exhibit non-linear behavior (where output doesn't change proportionally to input). ANNs, on the other hand, can learn complex relationships from data and adapt their control strategy accordingly.
- **Improved Disturbance Rejection:** PI controllers can be susceptible to external disturbances affecting the system's output. ANNs can be trained to recognize these disturbances and adjust the control signal to minimize their impact.
- **Set-point Tracking:** PI controllers might take time to reach and stabilize at a new desired set-point. ANNs can learn the system's dynamics and adjust

control signals for faster and smoother set-point transitions.

- **Generalization to Unseen Conditions:** PI controllers require manual tuning for different operating conditions. Properly trained ANNs can generalize their control strategy to situations not encountered during training, improving adaptability.
- **Multi-variable Control:** PI controllers are typically designed for single-input, single-output systems. ANNs can handle systems with multiple inputs and outputs, making them suitable for complex control problems.

3.2.4 Design Of ANN Based Internal Control Strategy

In the ANN Based Internal Control Strategy the PI controllers inside the voltage control loop is replaced by ANN controllers. Designing of an ANN controller mainly depends upon arranging the data required to train the ANN model. PI controllers used in the voltage control loop of the internal controller are used as supervisory controllers from which the necessary training data is extracted.

GCDCDG system is used as the plant. Inputs given to the ANN controller are the error inputs e_d and e_q as shown in block diagram given in Fig. 3.3. Similarly system outputs are u_d and u_q . For data collection both the ANN controllers were trained with the same test case data set for a fair comparative analysis.

In this context, 400,000 data samples of input and outputs of supervisory controllers were stored in lookup tables x and u , respectively. These training samples were obtained under a total of 4 dynamic test combinations to ensure comprehensive learning of ANN controllers.

1. GCDCDG subjected to grid frequency change.
2. GCDCDG subjected to grid voltage magnitude change.

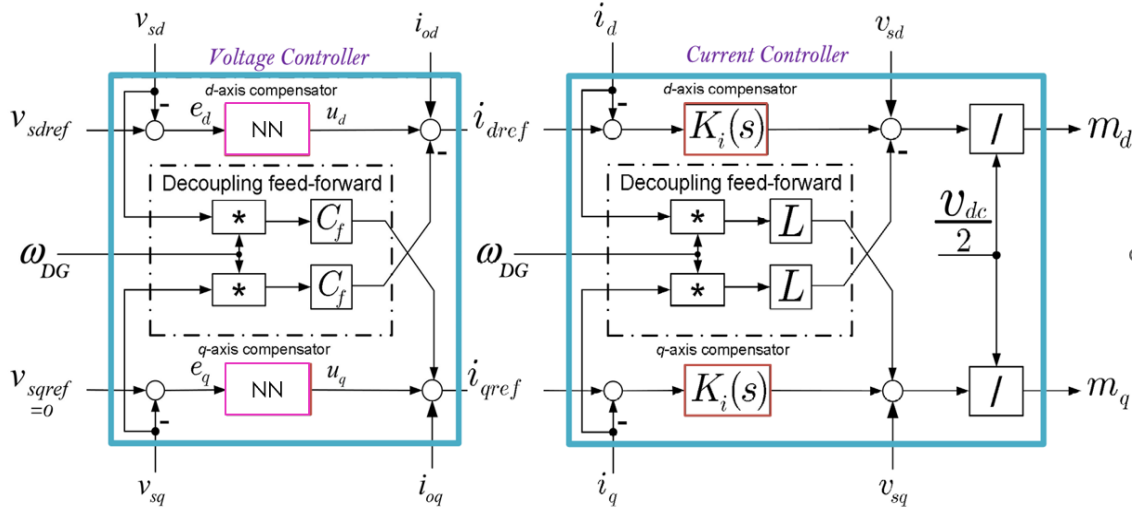


Figure 3.3: ANN based Internal Controller Strategy

3. GCDCDG subjected to both grid frequency and voltage magnitude change along with balanced load injection.
4. GCDCDG subjected to both grid frequency and voltage magnitude change along with unbalanced load injection.

Furthermore, each test case was executed for 1 s, with a time stamp of $1*10^{-5}$ s, resulting in 100000 data samples per case. So total samples collected is equal to $4*100,000 = 400,000$. These samples cover a wide range of dynamic scenarios that can possibly be encountered in a grid-connected VSC system. The collected data is then divided into 70% training, 15% validation, and 15% as testing for effective training.

The Levenberg–Marquardt-based backpropagation (LMBP) method is one of the fastest ANN training algorithms and it is used in this project to train all the ANN controllers. Training algorithm like LMBP adjusts the weights and biases within the neural network. This algorithm uses the collected data to minimize the error between the network's output and the desired control signal. The training algorithm

minimizes the cost function in the allowed epoch range N with respect to W(weight) and b(bias) to determine their updated values. Performance of the ANN controller depends upon assigning proper values to the weights and biases. Updating of weights and biases stop when the algorithm limits the cost function below a predetermined threshold value.

3.3 MPC Based Internal Controller

MPC (Model Predictive Controller) is based on the following basic concepts :

- A model is derived that describes the behaviour of the system. This model is then used to predict the system's behaviour over a predefined horizon length (number of time steps) into the future.
- A cost function represents the control objectives, and assigns a weighting to each objective. The cost is used to evaluate and compare the suitability of future actuation options.
- The actuation sequence that minimises the cost function is selected as the optimal solution. Only the first actuation of the optimal sequence is applied, discarding the rest of the sequence. Hereafter the process is repeated in order to re-evaluate the state and performance of the system resulting from this actuation. In this sense the prediction horizon is shifted forward in time along with the control actions applied at each new time step. The controller thus never applies the rest of the sequence predicted during a specific time step. This concept is known as the receding horizon principle.

The basic principles of MPC were developed in the 1960s and attracted interest from industry in the 1970s. Thereafter MPC has been applied in the chemical and process industries. The time constants were sufficiently long for calculations to be

completed. In the 1980s MPC was introduced in the power electronics industry in high-power applications with low switching frequencies. The control algorithm needed long calculation times therefore applications with high switching frequencies were not possible at the time. As the technology regarding microprocessors rapidly developed, MPC started to receive more interest due to increased computational capabilities being available.

3.3.1 Advantages of MPC

1. Multi-variable problems become simple.
2. It allows compensation of dead time.
3. The controller offers simple implementation for a wide variety of systems. There are many possibilities for adaptations and extensions to suit specific applications.
4. Non-linearities are easily included in the system model, eliminating the need to linearise it according to a specific operating point. This allows operation under any conditions. Variable restrictions can also be included in the design. Aside from MPC, this advantage is very challenging to implement in other types of predictive controllers such as deadbeat control.

3.3.2 Disdvantages of MPC

1. The computational complexity involved in evaluating and selecting the optimal solution candidate increases exponentially as the prediction horizon is lengthened further into the future. This can however be managed and mitigated by applying intelligent optimisation algorithms.

-
2. The controller is dependent on the system's model. Therefore the quality of the model derived for the system will determine the quality of the controller and its performance . If the system parameters change throughout time, an estimation or adaptation algorithm has to be incorporated.
 3. High computational burden and longer time consumption make it less attractive, especially in small-scale solar, wind energy applications, consumer electronics, low power embedded systems, and so on.

3.3.3 Design of MPC

Steps for implementing MPC:

1. State space modelling of the system
2. Discretization
3. Cost function formation
4. MPC program formation

Fig 3.4 represents the proposed system with MPC implementation. MPC replaces the earlier internal controller strategy.

3.3.4 State-Space Representation Of The Proposed System

- **State Variables:**

- I_{od} and I_{oq} (d and q components of the filter current)
- V_{od} and V_{oq} (d and q components of the filter capacitor voltage)

- **Control Variables:**

- S_a, S_b, S_c (Switching states of the inverter legs (0 or 1))

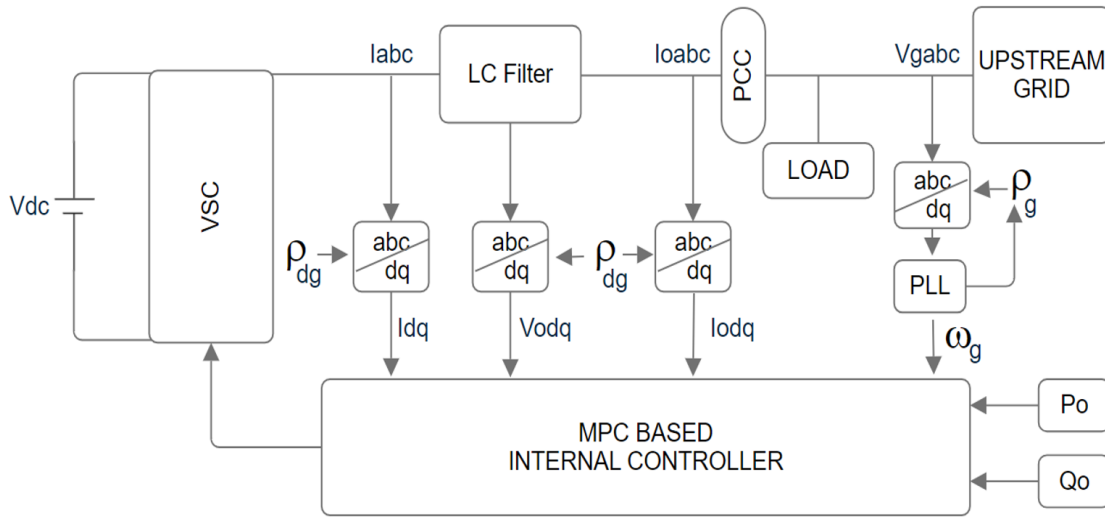


Figure 3.4: Proposed System With MPC

- Inverter has three legs, each leg contains two switches which are complementary. S_a, S_b, S_c represents each leg.

- **System Dynamics (in d-q frame):**

KVL theorem (after converting the system into d-q frame) is used to determine the equations required to model the proposed system.

$$\frac{dI_{od}}{dt} = \frac{1}{L}(-R * I_{od} + \omega * L * I_{oq} + \frac{2}{3 * V_{dc}} * S_a - V_{od}) \quad (3.1)$$

$$\frac{dI_{oq}}{dt} = \frac{1}{L}(-R * I_{oq} + \omega * L * I_{od} + \frac{2}{3 * V_{dc}} * S_b - V_{oq}) \quad (3.2)$$

$$\frac{dV_{od}}{dt} = \frac{1}{C}(I_{od} + \omega * C * V_{oq} + I_{gd}) \quad (3.3)$$

$$\frac{dV_{oq}}{dt} = \frac{1}{C}(I_{oq} + \omega * C * V_{od} + I_{gq}) \quad (3.4)$$

Where R, L, C are filter resistance, inductance and capacitance respectively. Equations (3.1), (3.2), (3.3), (3.4) are derived from KVL. Which is then converted into state space model as given below.

$$\frac{dx}{dt} = \mathbf{Ax} + \mathbf{Bu} \quad (3.5)$$

where,

$$\mathbf{A} = \begin{bmatrix} \frac{-R}{L} & \omega & \frac{-1}{L} & 0 \\ -\omega & \frac{-R}{L} & 0 & \frac{-1}{L} \\ \frac{1}{C} & -\omega C & 0 & 0 \\ \omega C & \frac{1}{C} & 0 & 0 \end{bmatrix}. \quad (3.6)$$

$$\mathbf{B} = \begin{bmatrix} \frac{2V_{dc}}{3L} & 0 & 0 \\ 0 & \frac{2V_{dc}}{3L} & 0 \\ 0 & 0 & \frac{2V_{dc}}{3L} \end{bmatrix}. \quad (3.7)$$

$$x = \begin{bmatrix} I_{od} \\ I_{oq} \\ V_{od} \\ V_{oq} \end{bmatrix} \quad (3.8)$$

$$u = \begin{bmatrix} S_a \\ S_b \\ S_c \end{bmatrix} \quad (3.9)$$

3.3.5 Cost Function

Cost function is designed to limit the I_{od} and I_{oq} currents, by minimising the difference between it and reference currents I_{odref} and I_{oqref} . Cost function is given as:

$$g = (I_{od} - I_{odref})^2 + (I_{oq} - I_{oqref})^2$$

3.3.6 MPC Main Program

The flowchart shown in Fig 3.5 represents the main algorithm displaying MPC functionality. System model is first discretized, then inner for loop minimises

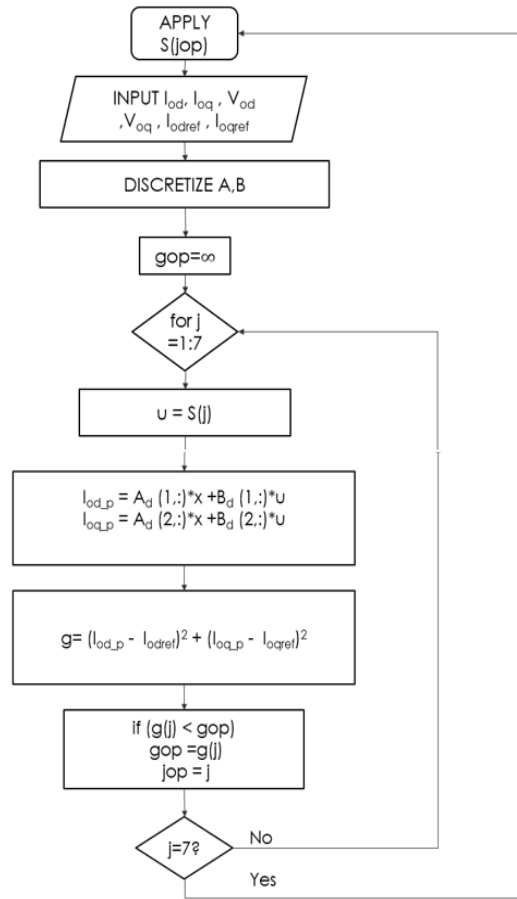


Figure 3.5: MPC Main Algorithm

the cost function and finds the best possible switching combination for each time step. The outer loop ensures that this procedure continues till the simulation stops. Here the prediction horizon is one time step. If more than one time step is taken the MPC program would be highly complex and would require lot computation time for a slight increase in performance.

4 Simulation, Results and Discussions

This chapter is divided into three sections. The first section consists of the implementation of the proposed droop control strategy on the GCDCDG. The second section focuses on the implementation of ANN controllers on the internal controller of the GCDCDG. The third section concentrates on the implementation of MPC based internal controller for the the GCDCDG. In all three sections several case studies are performed to establish the viability of all the control strategies proposed in this project work.

4.1 Implementation Of The Proposed Droop Control Strategy

In this section, the performance of the proposed strategy is investigated under six different case studies. The proposed droop-control based power and current limiting strategy is applied to a GCDCDG. The detailed model of the system is simulated using MATLAB/Simulink environment. The main simulation diagram is shown in fig 4.1 in which the upstream grid is represented by a series

inter-link line connected in series with ideal voltage source.

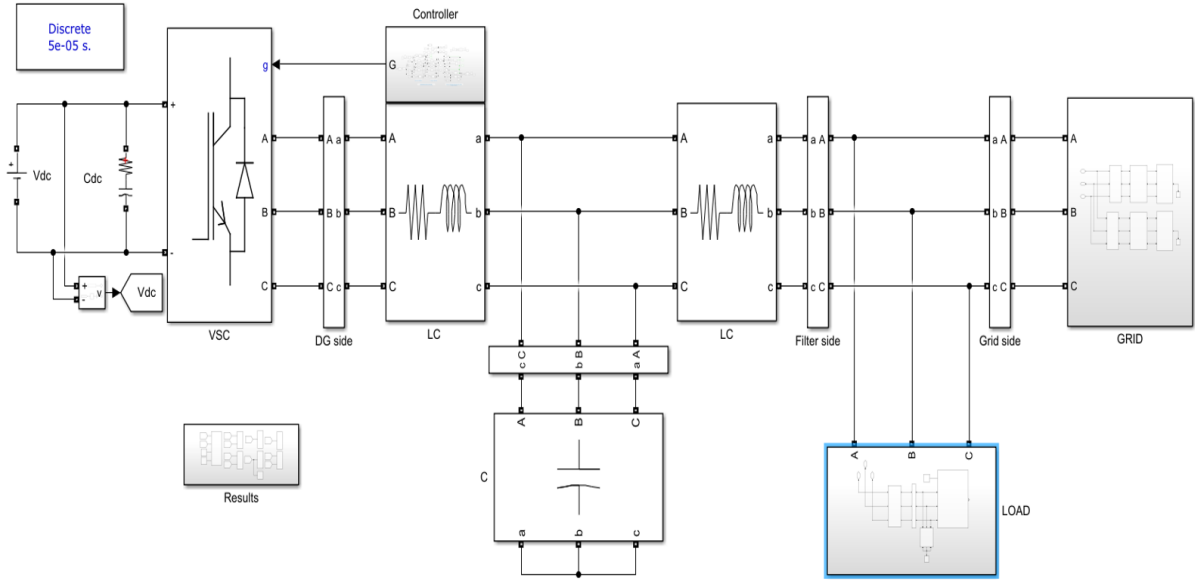


Figure 4.1: Main Simulation Diagram

In all cases, until $t = 2$ sec, DG operates in its initial conditions, which are $V_{od} = 51$ V, $f_0 = 50$ Hz, $P_0 = 235$ W, $Q_0 = 59.6$ VAr, $i_{od} = 3.068$ A and $i_{od} = 0.779$ A. Also, the line to line voltage of UG is 61.24 V.

Fig 4.2 represents the internal controller without proposed droop control strategy. While Fig 4.3 represents the internal controller with proposed droop control strategy. Both cases are implemented and same test cases are performed in both of them, so that we can directly compare the results and look into the benefits of implementing the proposed droop control strategy. Parameters of this DG are given in the table below.

Parameter	Symbol	Value
Rated power	S_n (kVA)	1.1
Rated voltage	V_n (V)	50
DC bus voltage	V_{DC} (V)	200
Rated frequency	f_0	50
Switching frequency	f_{SW} (kHz)	20
Filter inductance	L_f (mH)	1.5
Filter capacitance	C_f (μ F)	20
Filter resistance	R_f (m Ω)	1.5
Rated active power	P_0 (W)	240
Rated reactive current	Q_0 (W)	60
Maximum active current	i_{odmax} (A)	12
Minimum reactive current	i_{qdmax} (A)	-7.2
Active power droop coefficient	m_d	0.001
Reactive power droop coefficient	n_q	0.002
PI controller proportional gain of active current	K_{P-id}	0.4
PI controller integral gain of active current	K_{I-id}	0.5
PI controller proportional gain of reactive current	K_{P-iq}	-4
PI controller integral gain of reactive current	K_{I-iq}	-5
LPF cut-off frequency	ω (rad/s)	15
Interlink line resistance	R_L (Ω)	0.001
Interlink line inductance	L_L (mH)	0.001

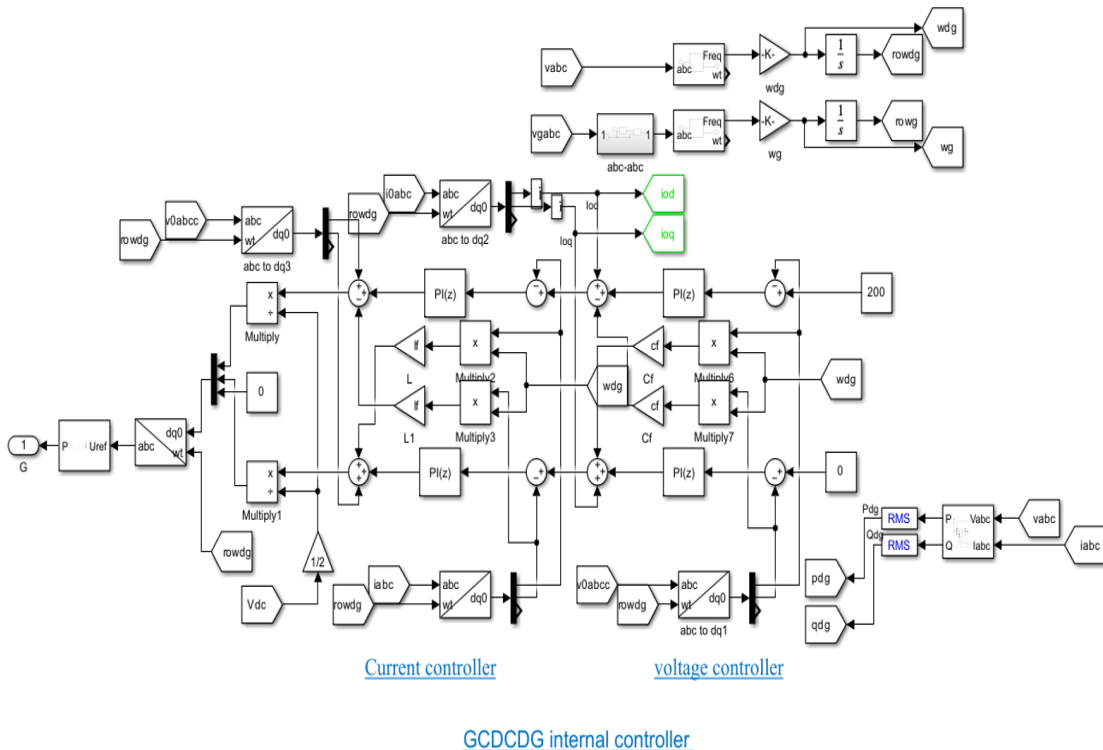


Figure 4.2: GCDCDG Controller Without Proposed Strategy

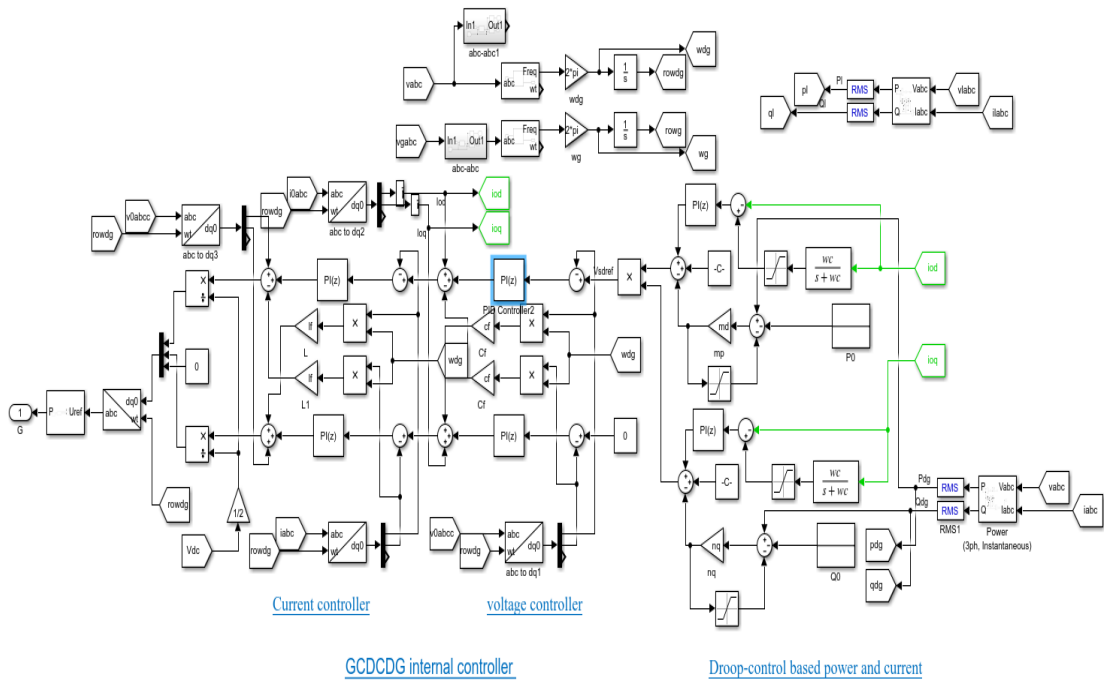


Figure 4.3: GCDG Controller With Proposed Strategy

4.1.1 Case 1: UG Frequency Drop Without Proposed Strategy

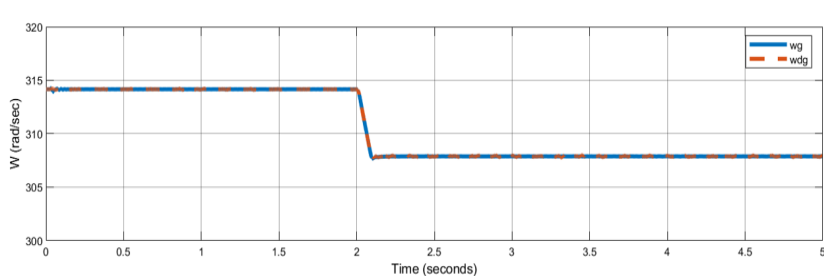


Figure 4.4: DG, Grid Frequency vs Time

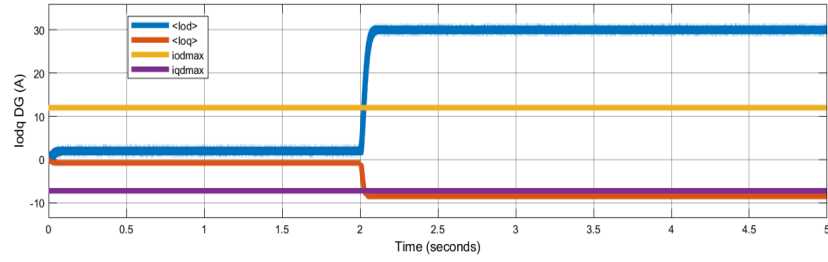


Figure 4.5: Output dq Currents vs Time

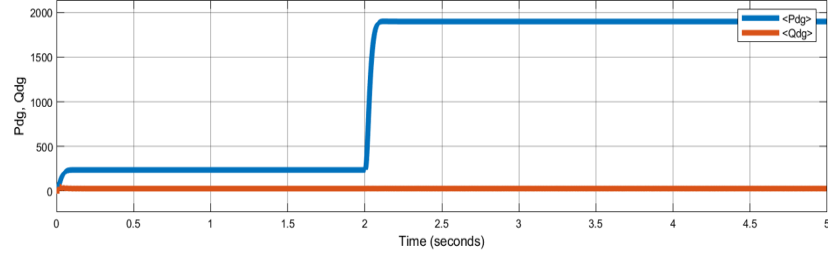


Figure 4.6: Output Active and Reactive Power vs Time

Inference

The effect of grid frequency change in the system is studied in both case 1 and case 2. It is done by applying a step change in grid frequency by 1 Hz. So at $t = 2$ sec the UG frequency drops to 49Hz from 50Hz. Active power injection from DG to UG begins to increase, as a result i_{od} starts increasing as well. 1Hz Frequency drop is large and i_{od} exceeds the maximum specified limit if the current limiting strategy is not used. Also, the injected active power reaches about 1900W which is greater than the rated power of the DG.

4.1.2 Case 2: UG Frequency Drop With Proposed Strategy

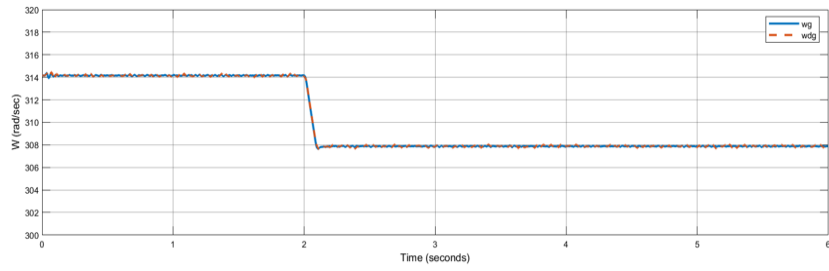


Figure 4.7: DG, Grid Frequency vs Time

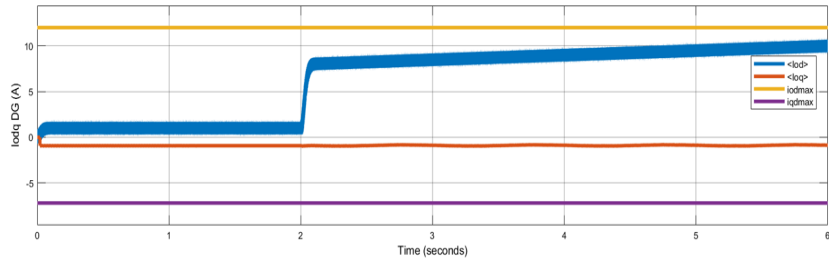


Figure 4.8: Output dq Currents vs Time

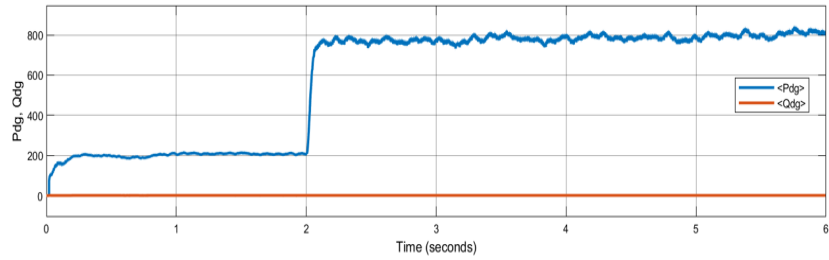


Figure 4.9: Output Active And Reactive Power vs Time

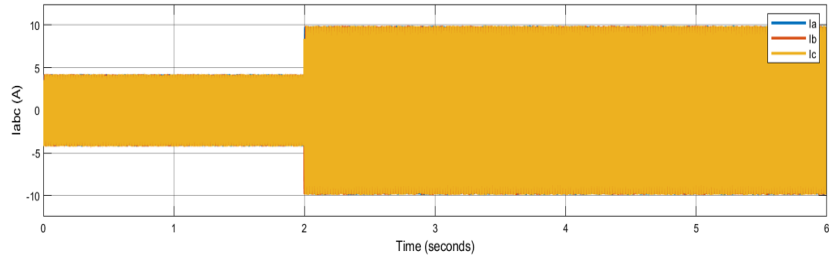


Figure 4.10: Output abc Currents vs Time

Inference

Same test scenario is performed here as seen in the earlier case. But here the proposed droop control is implemented in the system. With proposed strategy values of i_{od} and i_{oq} are within limits. Value of Active Power output is decreased from a peak value of 1900W to 800W. Tabular illustration of inference is given below.

PARAMETERS	WITHOUT PROPOSED STRATEGY	WITH PROPOSED STRATEGY
Change in Frequency	50 to 49 Hz	50 to 49 Hz
I_{od}	30A	Under 12A
Active power	1900W	800W

4.1.3 Case 3: UG Voltage Magnitude Drop Without Proposed Strategy

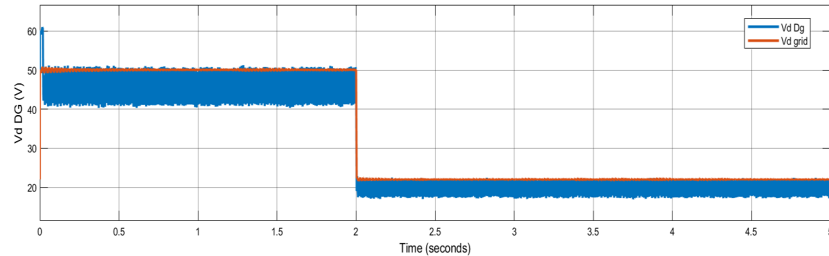


Figure 4.11: DG, Grid Voltage vs Time

Inferences: The effect of grid voltage magnitude change in the system is studied in both case 3 and case 4. In this case at $t = 2$ sec the UG voltage magnitude drops to 22.5 V from 50 V i.e. 55% decrease at PCC. i_{oq} exceeds

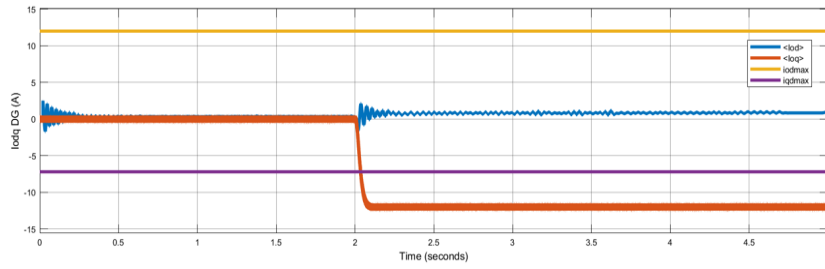


Figure 4.12: Output dq Currents vs Time

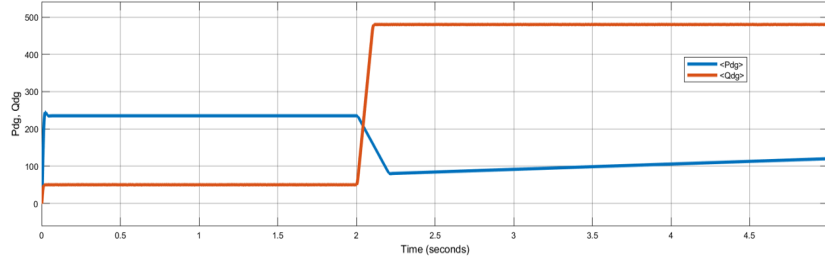


Figure 4.13: Output Active and Reactive Power vs Time

boundary and decreases to about -12A, if proposed strategy is not implemented. Because of this reactive current decreases, reactive power injection increases.

4.1.4 Case 4: UG Voltage Magnitude Drop With Proposed Strategy

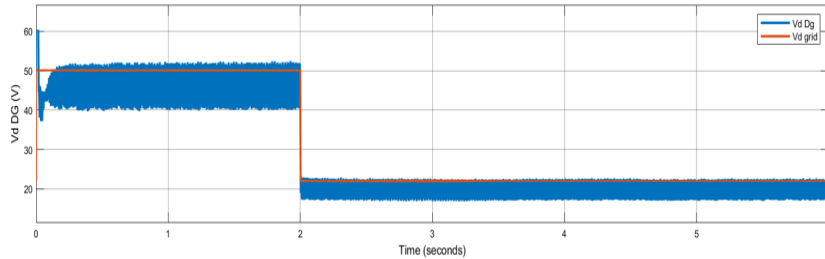


Figure 4.14: DG, Grid Voltage vs Time

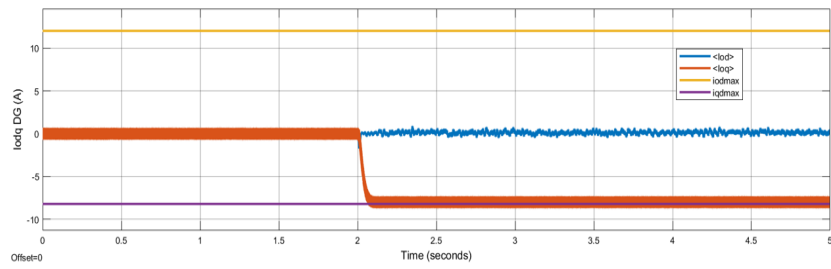


Figure 4.15: Output dq Currents vs Time

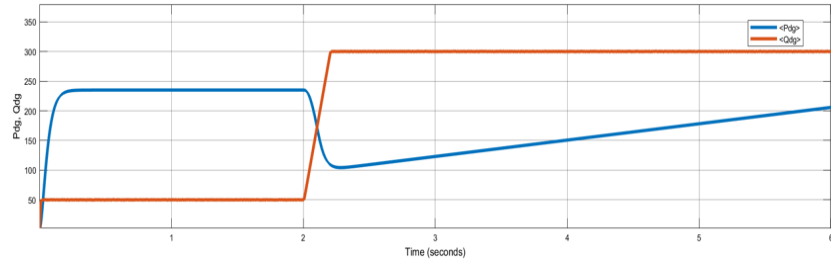


Figure 4.16: Output Active and Reactive Power vs Time

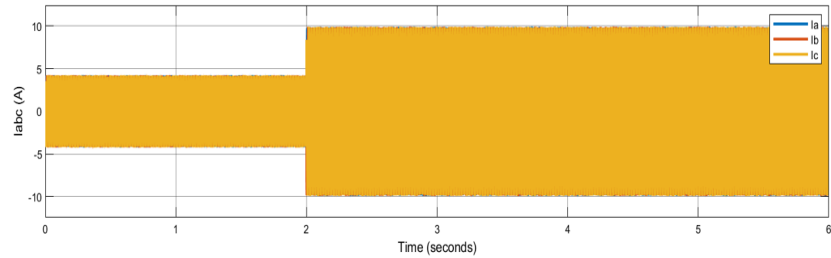


Figure 4.17: Output abc Currents vs Time

Inferences:

With the proposed strategy values of i_{od} and i_{oq} are within limits. Value of Reactive Power output is decreased from a peak value of 480 Vars to 300 Vars. Tabular illustration of inference is given below.

PARAMETERS	WITHOUT PROPOSED STRATEGY	WITH PROPOSED STRATEGY
Change in Grid Voltage Magnitude	50 to 22.5 V	50 to 22.5 V
I_{oq}	-12 A	-7.2 A
Reactive Power	480 Vars	300 Vars

4.1.5 Case 5: UG Frequency And Voltage Magnitude Drop With Balanced Load Injection

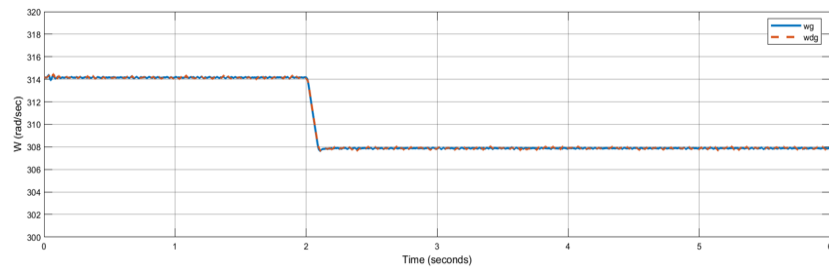


Figure 4.18: DG, Grid Frequency vs Time

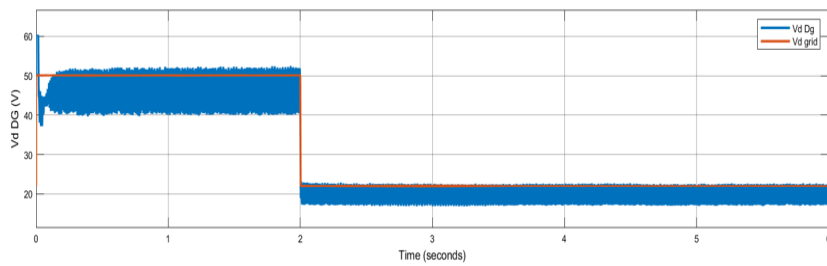


Figure 4.19: DG, Grid Voltage vs Time

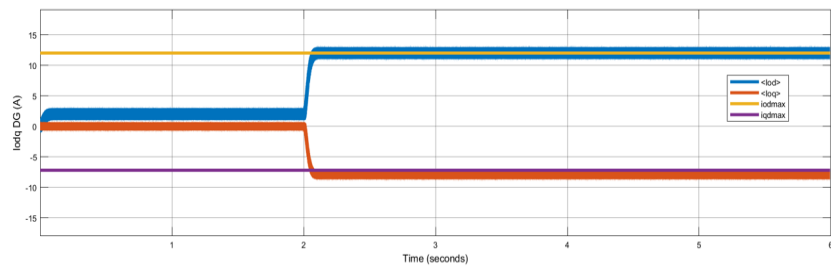


Figure 4.20: Output dq Currents vs Time

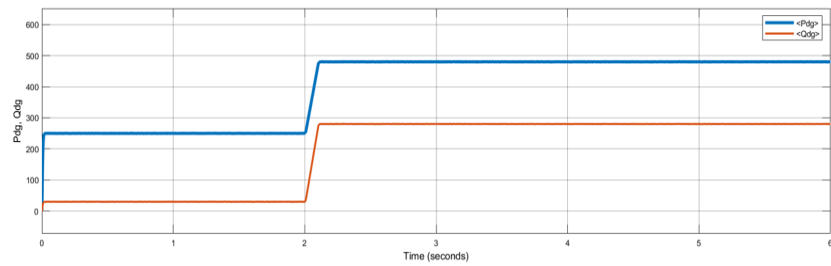


Figure 4.21: Output Active and Reactive Power vs Time

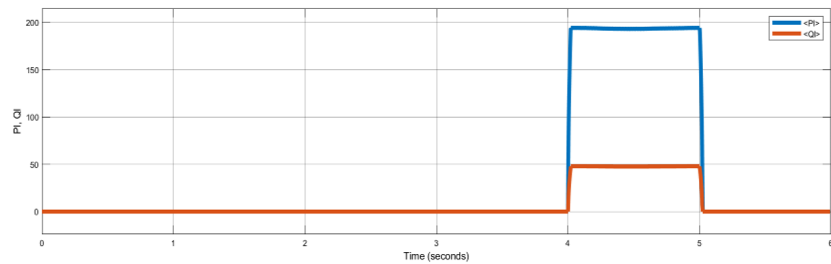


Figure 4.22: Active and Reactive Components of Balanced Load vs Time

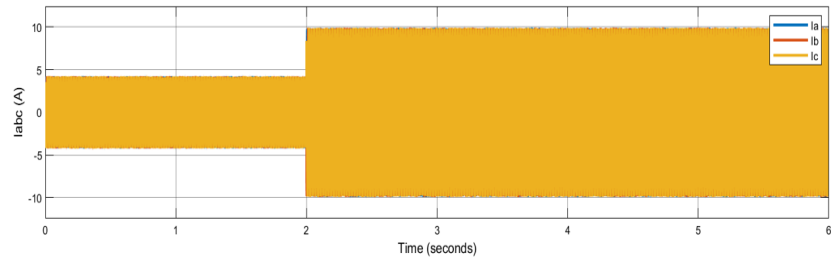


Figure 4.23: Output abc Currents vs Time

Inference:

To show the ability of the proposed current limiting strategy, UG frequency and voltage magnitude are simultaneously decreased to 49Hz from 50Hz and V_{dgrid} to 22.5 V from 50 V respectively. After $t = 2$ sec, when frequency and voltage magnitude are decreased, i_{od} and i_{oq} move to boundary values and in steady-state reaches to active and reactive powers of 471 W and 293 VAr, respectively. Between $t = 4$ sec and $t = 5$ sec, a three phase balanced load ($P_L = 174$ W and $Q_L = 45$ VAr) is connected at PCC and starts to draw current. Output currents of the DG are controlled and do not exceed boundary values, and are limited under the proposed strategy. The required power of the load is provided from the grid under this abnormal condition. Tabular illustration of the inference is given below.

PARAMETERS	VALUE AFTER $t = 2$ SEC	INFERENCE
I_{od}	12 A	Within limits
I_{oq}	-7.2 A	Within limits
P_{dg}	471 W	N/A
Q_{dg}	293 VAr	N/A

4.1.6 Case 6: UG Frequency And Voltage Magnitude Drop With Induction Motor Load Switching

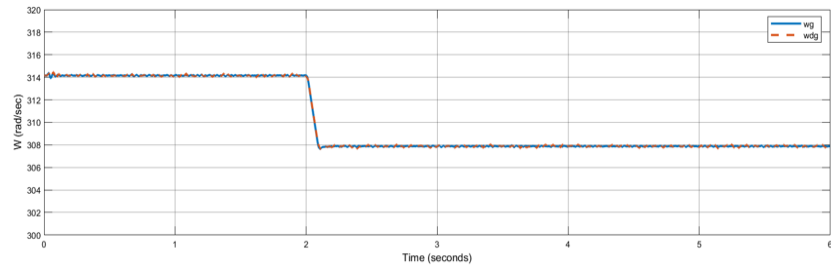


Figure 4.24: DG, Grid Frequency vs Time

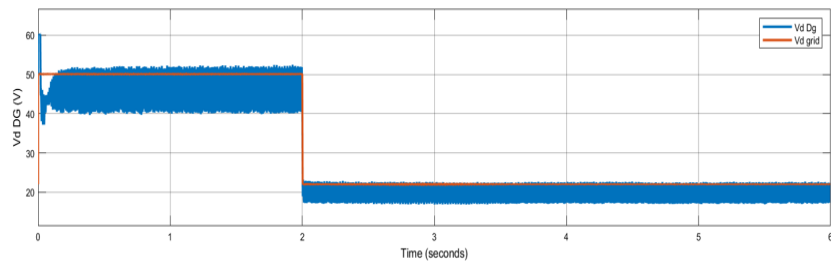


Figure 4.25: DG, Grid Voltage vs Time

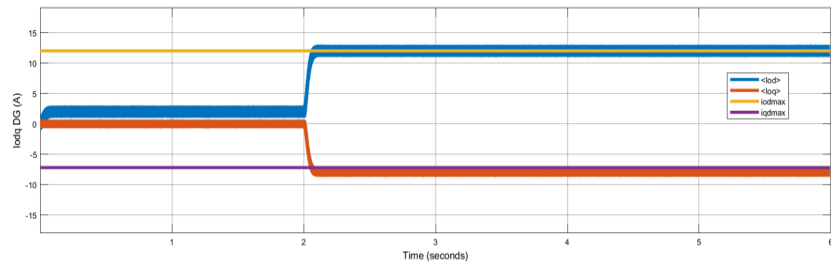


Figure 4.26: Output dq Currents vs Time

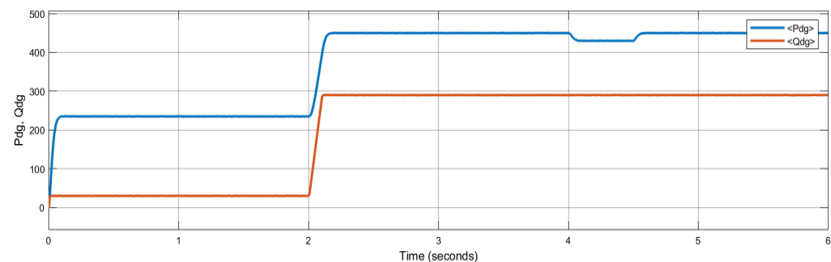


Figure 4.27: Output Active and Reactive Power vs Time

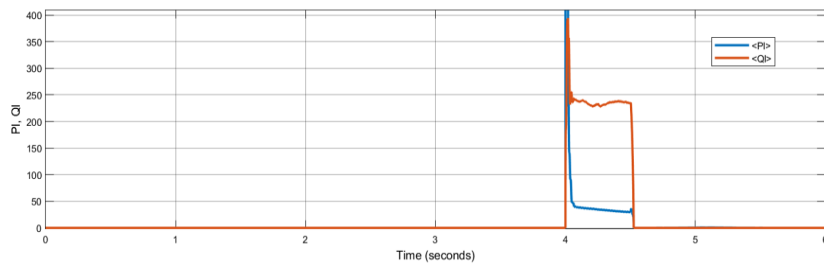


Figure 4.28: Active and Reactive Components of Induction Motor Load vs Time

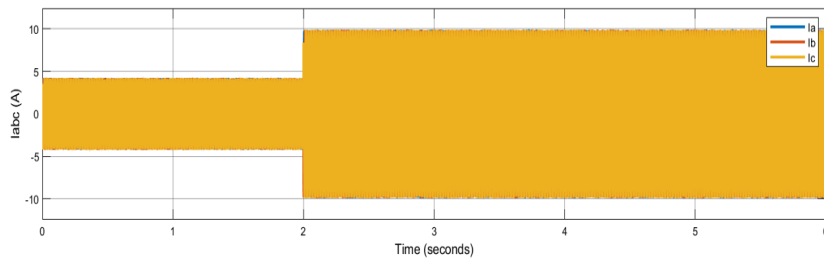


Figure 4.29: Output abc Currents vs Time

Inference:

This case study is the same as case study 5, but instead of a three-phase balanced load, an induction motor with $S = 200$ VA as a dynamic load is connected at $t = 4$ sec. Results show that the proposed strategy control the output currents and does not permit the currents to rise over the boundary values. Tabular illustration of the inference is given below.

PARAMETERS	VALUE AFTER $t = 2$ Sec	INFERENCE
I_{od}	12 A	Within limits
I_{oq}	-7.2 A	Within limits
P_{dg}	471 W	N/A
Q_{dg}	293 VAr	N/A

4.2 Implementation Of ANN Based Controller

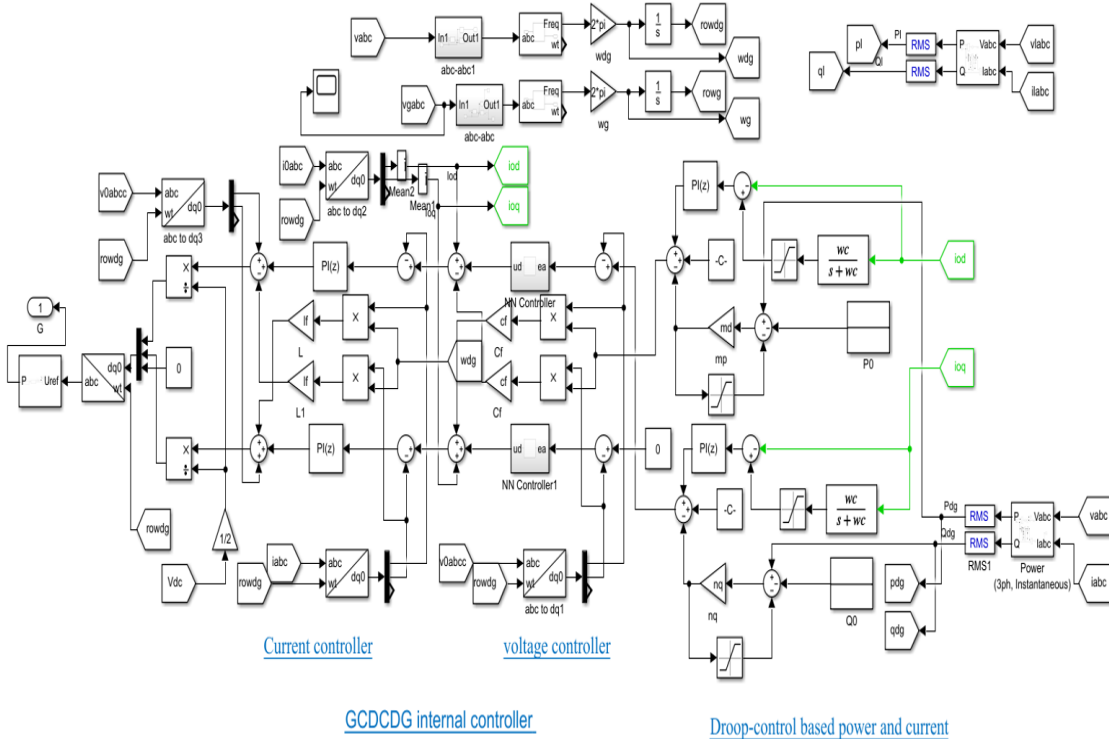


Figure 4.30: GCDCDG Controller With Proposed Strategy and ANN

In this section ANN controller is implemented in the outer loop of the internal controller. Superiority of ANN based controller over PI controller is checked with different case studies. There are 4 different cases covered here which are similar to the earlier section. Fig 4.30 represents the internal controller with ANN controller. The initial conditions and parameters used are same as the ones mentioned in the earlier section.

4.2.1 Case 1: UG Frequency Drop

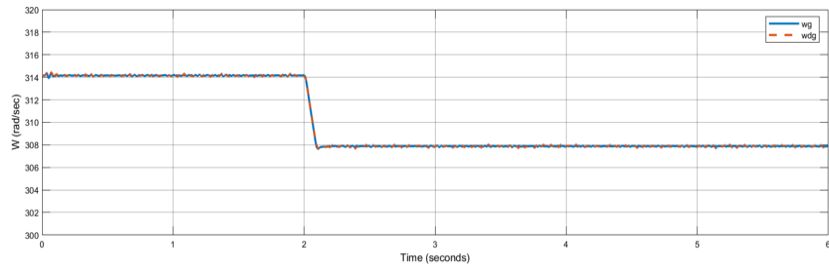


Figure 4.31: DG, Grid Frequency vs Time

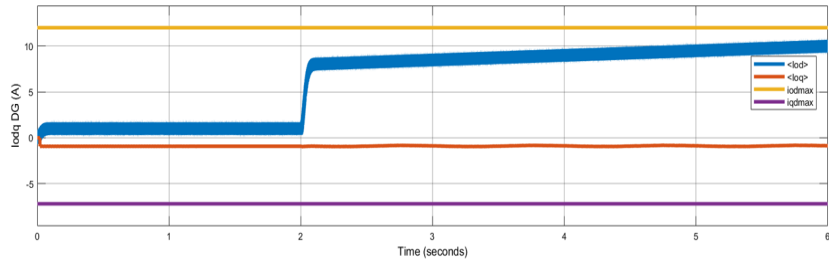


Figure 4.32: Output dq Currents vs Time(PI)

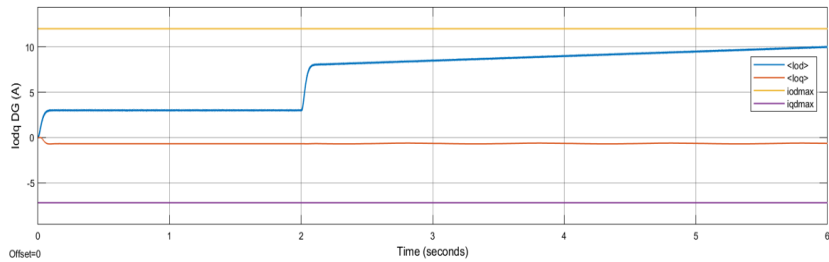


Figure 4.33: Output dq Currents vs Time(ANN)

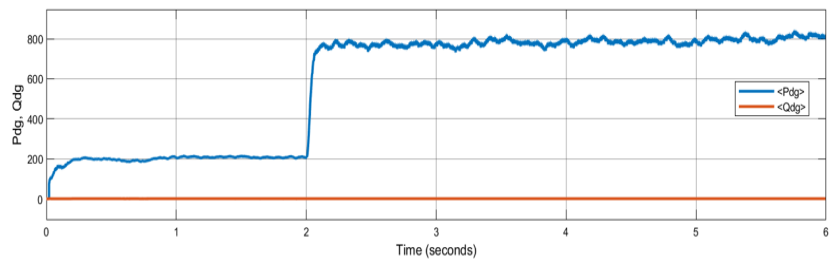


Figure 4.34: Output Active and Reactive Power vs Time (PI)

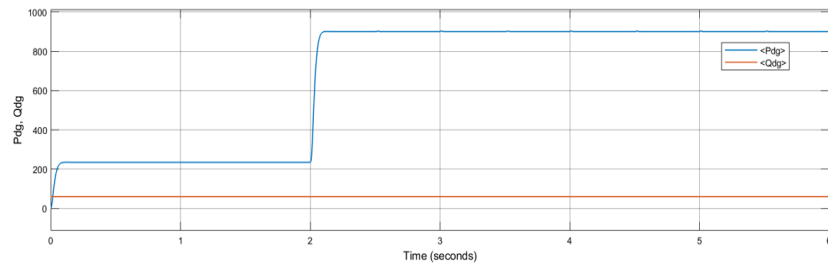


Figure 4.35: Output Active and Reactive Power vs Time (ANN)

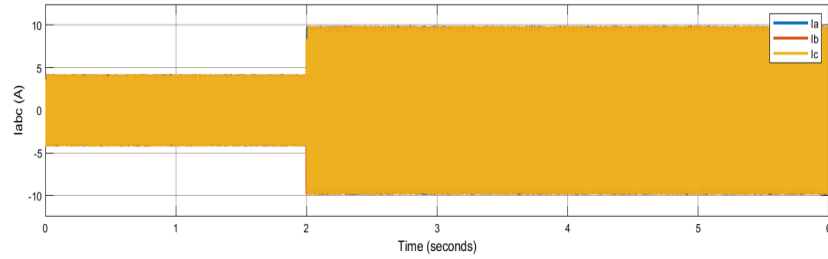


Figure 4.36: Output abc Currents vs Time(PI)

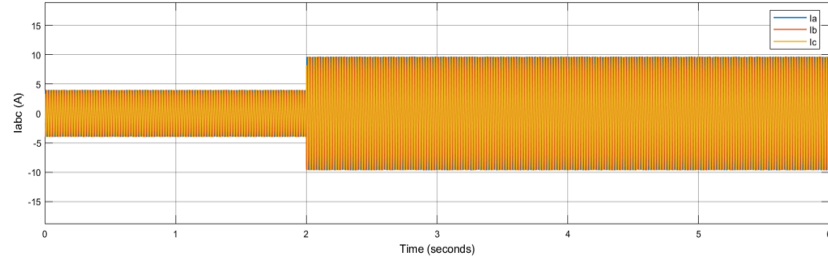


Figure 4.37: Output abc Currents vs Time(ANN)

Inference: This case is similar to case 1 and 2 in section 4.1. Here also the effect of UG frequency drop is studied for the proposed system with ANN controller. At $t = 2$ sec, UG frequency drops from 50 to 49 Hz. ANN based controller also performs current and power limiting properties as evident from waveforms. When waveforms of ANN based controller and PI based controller is compared head to head, we can observe that noise levels in both i_{od} and Active power is significantly less in ANN based GCDCDG when compared to

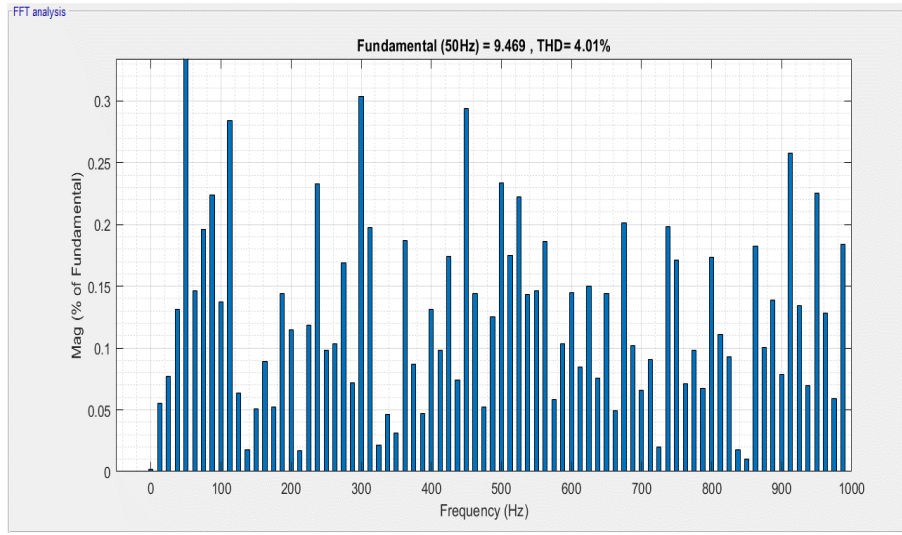


Figure 4.38: PI Based GCDCDG

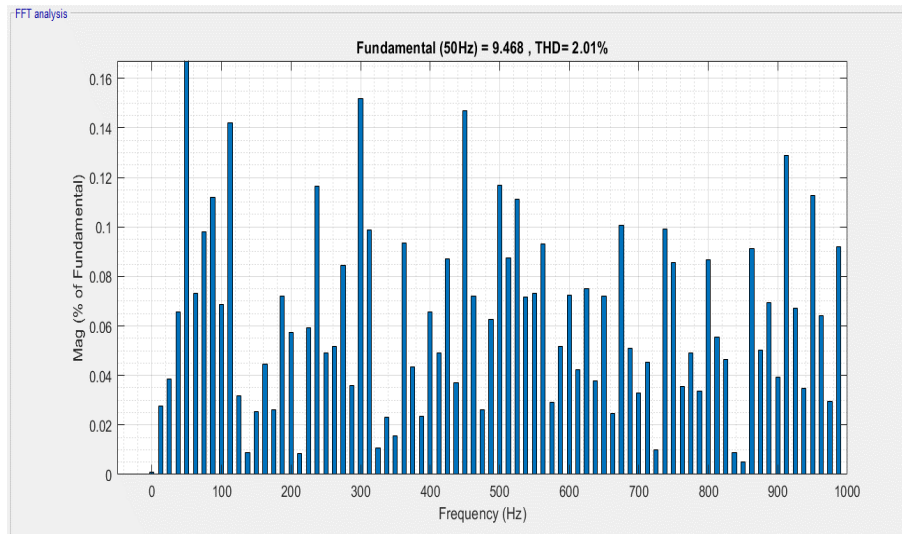


Figure 4.39: ANN Based GCDCDG

PI based GCDCDG . THD (of output abc current), Rise time (of i_{od}) have also improved in ANN based GCDCDG when compared to PI based. Tabular illustration is given below. Fig 4.38 and Fig 4.39 represents THD of both PI and ANN based GCDCDG.

PARAMETERS	PI BASED GCDCDG	ANN BASED GCDCDG
THD % OF GRID CURRENT @ $t = 3$ sec	4.01 %	2.01%
RISE TIME (I_{od})	40.931 ms	36.082 ms

4.2.2 Case 2: UG Voltage Magnitude

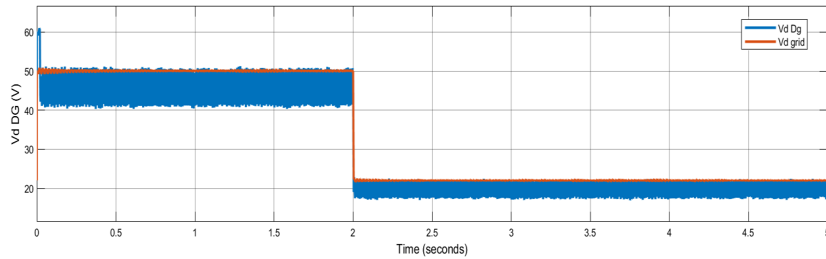


Figure 4.40: DG, Grid Voltage vs Time

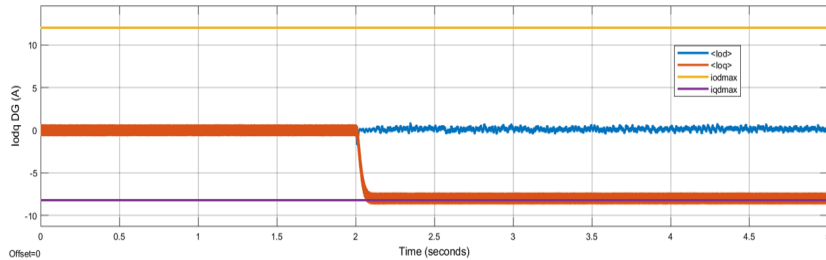


Figure 4.41: Output dq Currents vs Time (PI)

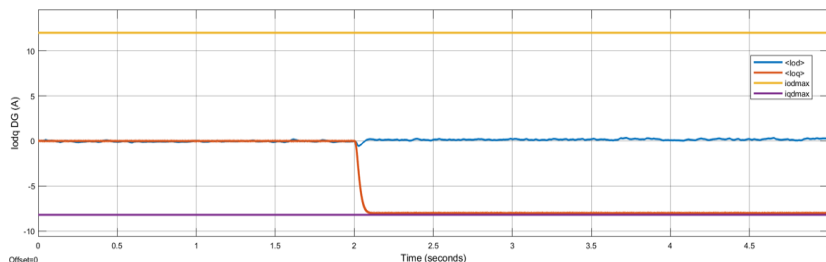


Figure 4.42: Output dq Currents vs Time (ANN)

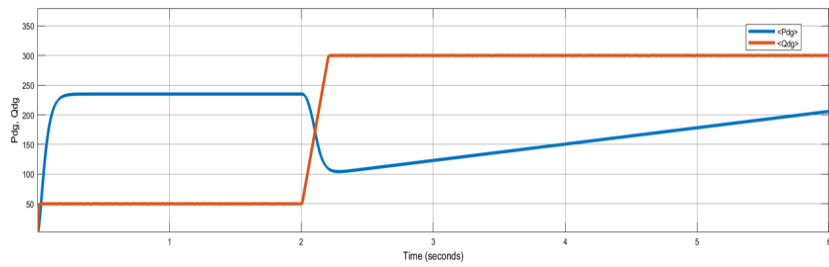


Figure 4.43: Output Active and Reactive Power vs Time(PI)

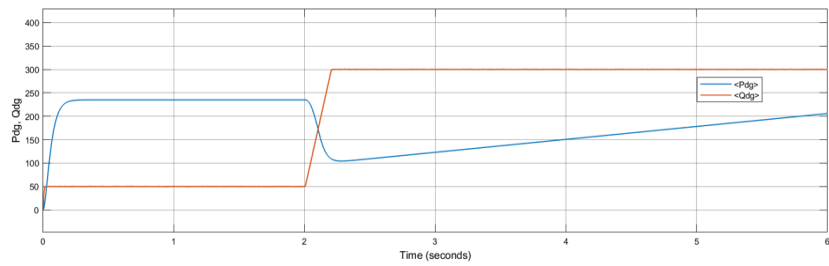


Figure 4.44: Output Active and Reactive Power vs Time(ANN)

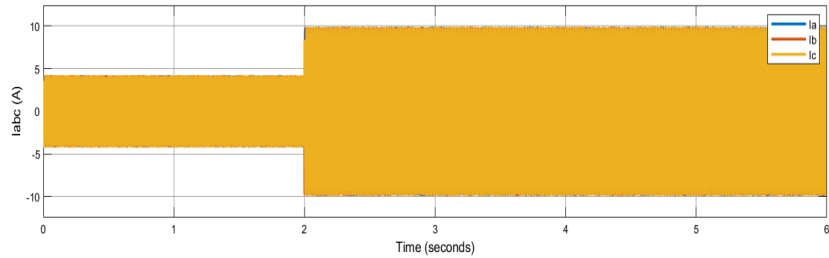


Figure 4.45: Output abc Current VS Time(PI)

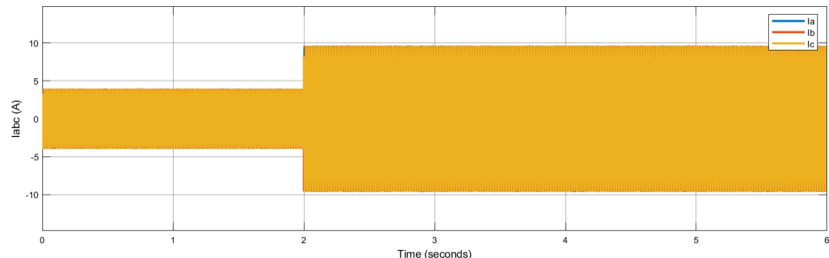


Figure 4.46: Output abc Current VS Time(ANN)

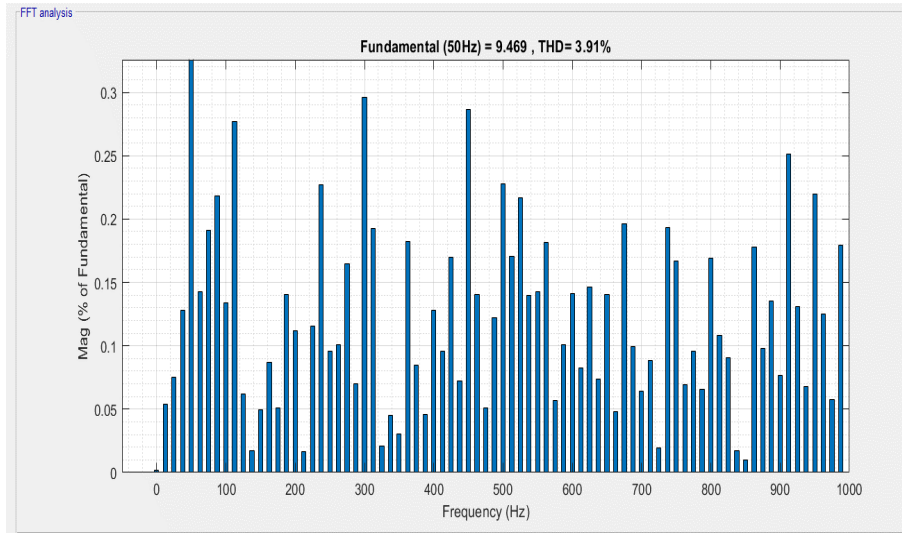


Figure 4.47: PI Based GCDCDG

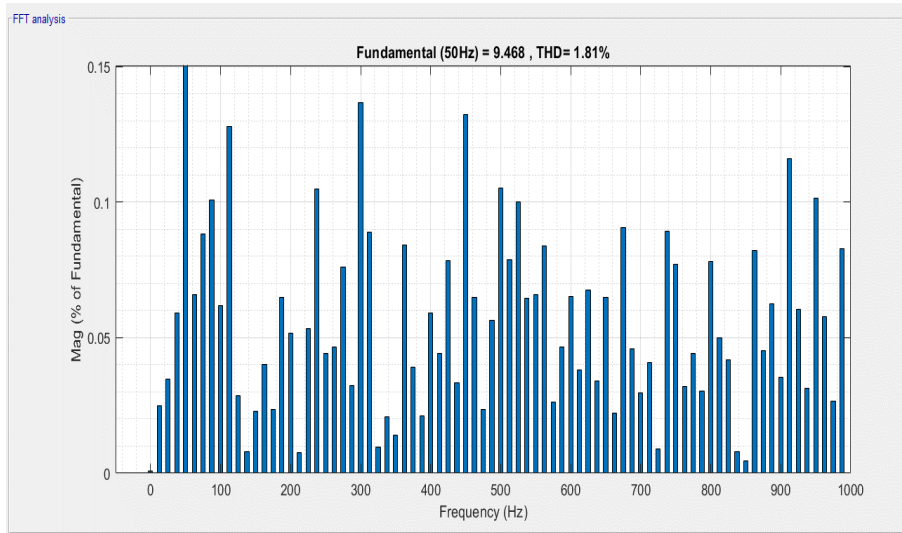


Figure 4.48: ANN Based GCDCDG

Inference: This case is similar to case 3 and 4 in section 4.1. Here also the effect of UG voltage magnitude drop is studied for the proposed system with ANN controller. In this case at $t = 2$ sec the UG voltage magnitude drops to 22.5 V from 50 V i.e. 55% decrease at PCC. ANN based controller also performs current and power limiting properties as evident from waveforms.

When waveforms of ANN based controller and PI based controller is compared head to head, we can observe that noise levels in both i_{oq} and reactive power is significant less in ANN based GCDCDG when compared to PI based GCDCDG as we can clearly observe from the waveforms above. THD (of output abc currents), Fall time (i_{oq}) have also improved in ANN based GCDCDG when compared to PI based. Tabular comparison of the results of both controllers are given below.

PARAMETERS	PI BASED GCDCDG	ANN BASED GCDCDG
THD % OF GRID CURRENT @ $t = 3$ sec	3.91 %	1.81%
FALL TIME (i_{oq})	42.174 ms	36.442 ms

4.2.3 Case 3: UG Frequency And Voltage Magnitude Drop With Balanced Load Injection

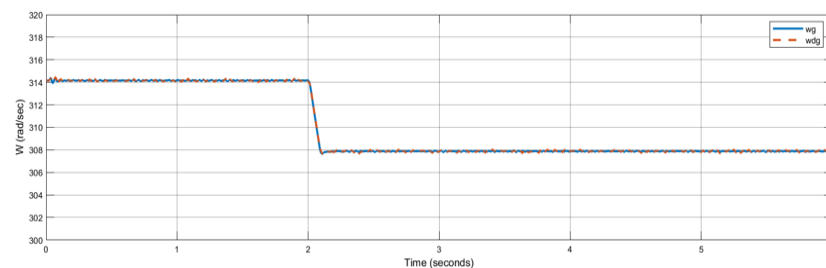


Figure 4.49: DG, Grid Frequency vs Time

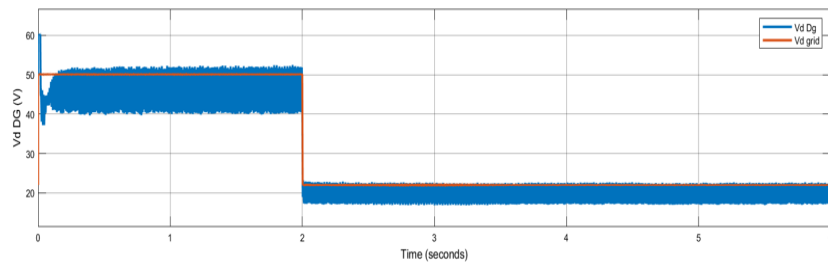


Figure 4.50: DG, Grid Voltage vs Time

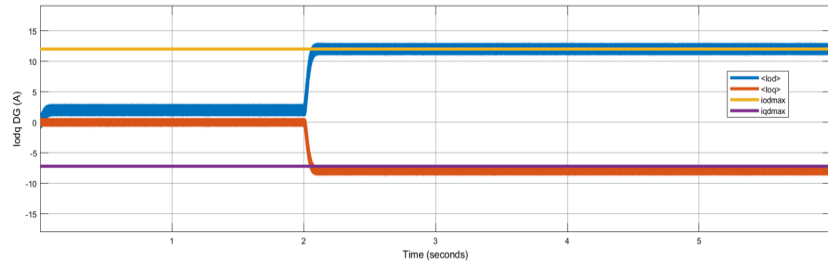


Figure 4.51: Output dq Currents vs Time(PI)

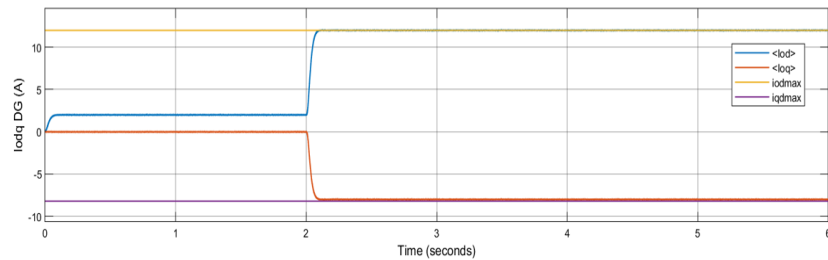


Figure 4.52: Output dq Currents vs Time(ANN)

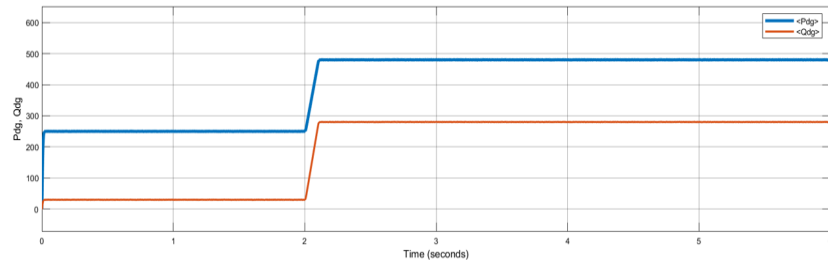


Figure 4.53: Output Active and Reactive Power vs Time(PI)

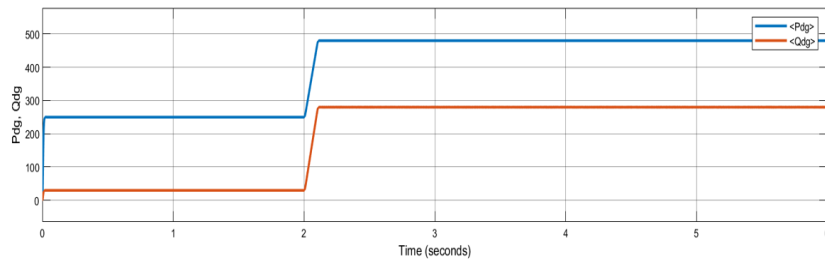


Figure 4.54: Output Active and Reactive Power vs Time(ANN)

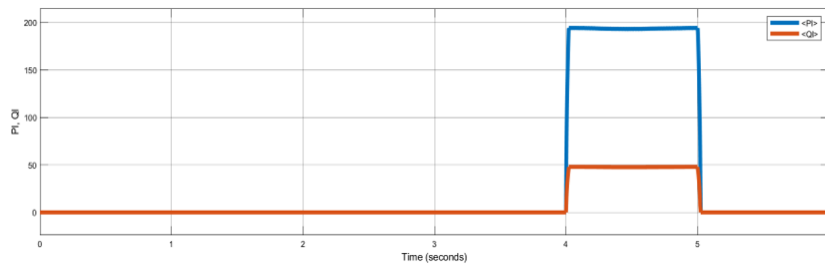


Figure 4.55: Active and Reactive Components of Balanced Load vs Time

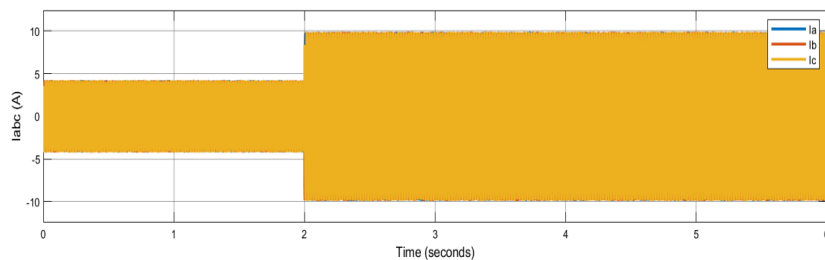


Figure 4.56: Output abc Currents vs Time (PI)

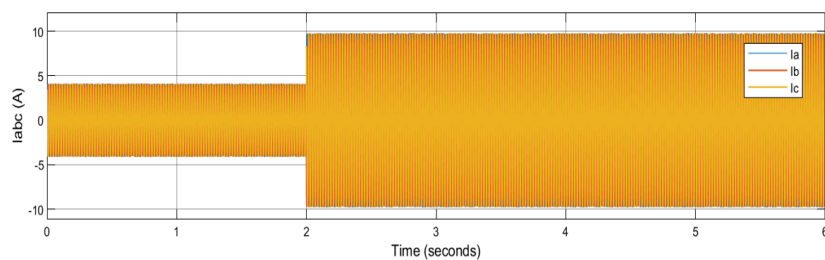


Figure 4.57: Output abc Currents vs Time (ANN)

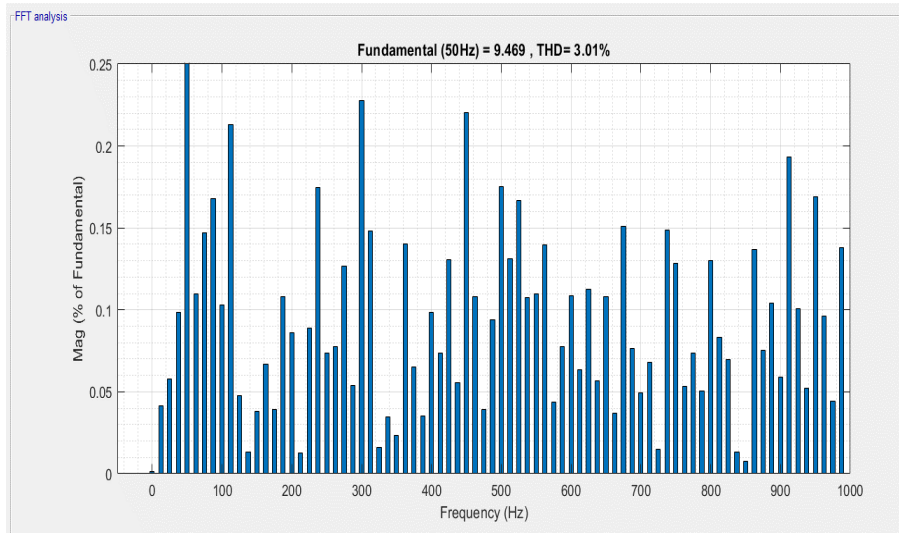


Figure 4.58: PI Based GCDCDG

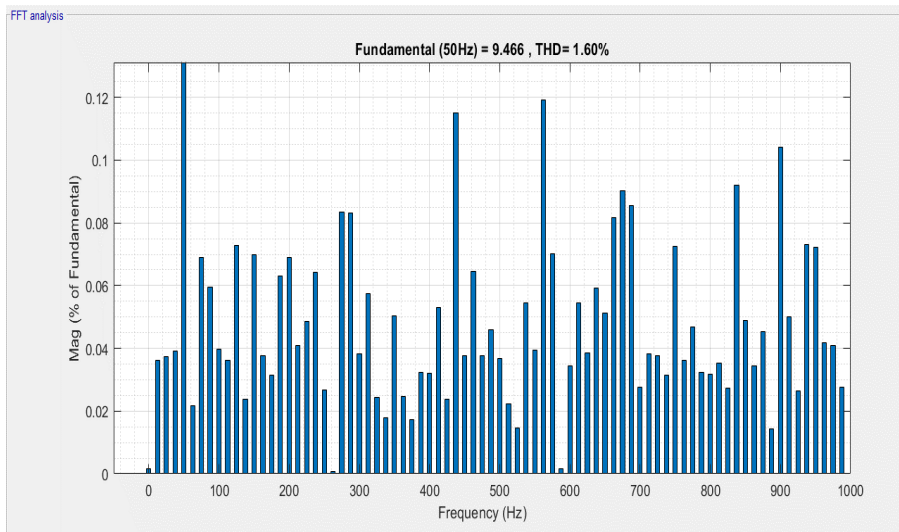


Figure 4.59: ANN Based GCDCDG

Inference:

This case is similar to case 5 in section 4.1. Here also the effect of simultaneous UG voltage magnitude and frequency drop is studied for the proposed system with ANN controller. In this case at $t = 2$ sec the UG voltage magnitude drops to 22.5 V from 50 V (i.e. 55% decrease at PCC) along with that

UG grid frequency also drops from 50 to 49 Hz. Between $t = 4$ sec and $t = 5$ sec, a three phase balanced load ($P_L = 174$ W and $Q_L = 45$ VAr) is also connected at PCC. ANN based controller also performs current and power limiting properties as evident from waveforms. When waveforms of ANN based controller and PI based controller is compared head to head, we can observe that noise levels in i_{od} , i_{oq} . Active and Reactive power is significantly less in ANN based GCDCDG as we can clearly observe from the figures waveforms. THD (of output abc currents), Rise time (of i_{od}) and fall time (of i_{oq}) have also improved in ANN based GCDCDG when compared to PI based.

PARAMETERS	PI BASED	ANN BASED
THD % OF GRID CURRENT @ $t = 3$ sec	3.01 %	1.60 %
RISE TIME (I_{od})	45.576 ms	36.790 ms
FALL TIME (I_{oq})	44.693 ms	34.096 ms

4.2.4 Case 4: UG Frequency And Voltage Magnitude Drop With Induction Motor Load Switching

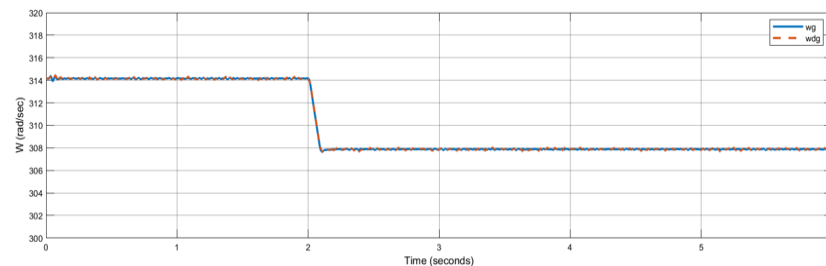


Figure 4.60: DG, Grid Frequency vs Time

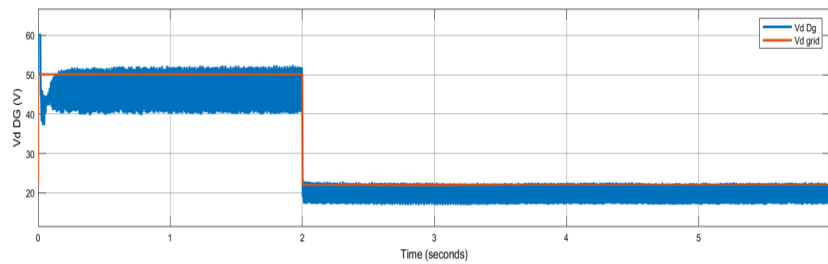


Figure 4.61: DG, Grid Voltage vs Time

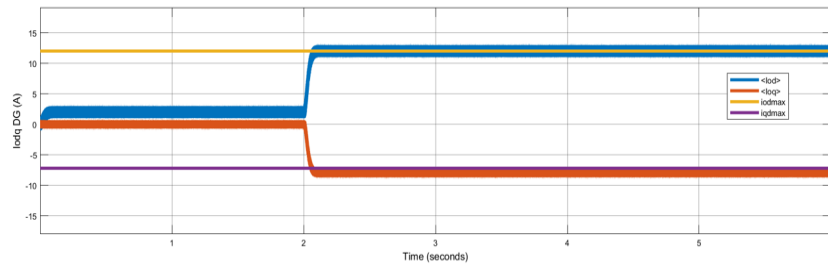


Figure 4.62: Output dq Currents vs Time(PI)

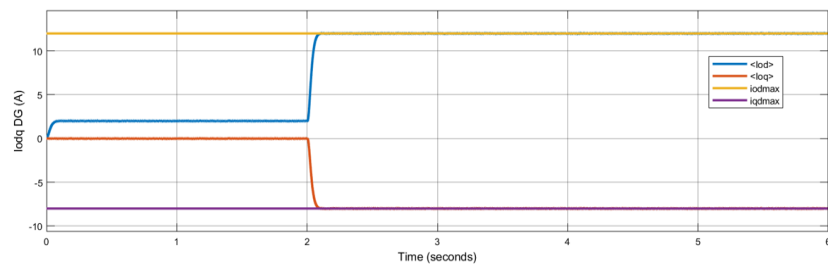


Figure 4.63: Output dq Currents vs Time(ANN)

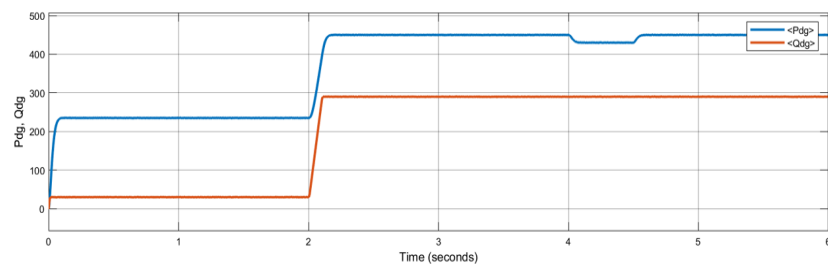


Figure 4.64: Output Active and Reactive Power vs Time(PI)

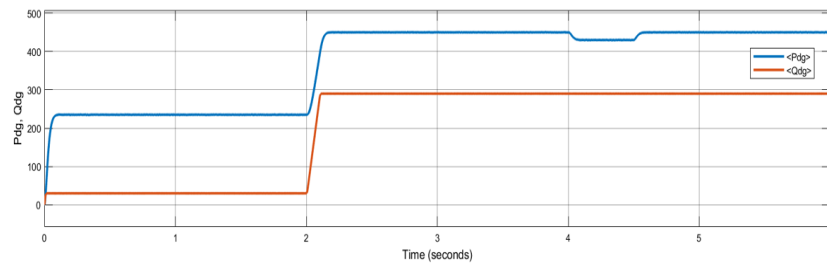


Figure 4.65: Output Active and Reactive Power vs Time(ANN)

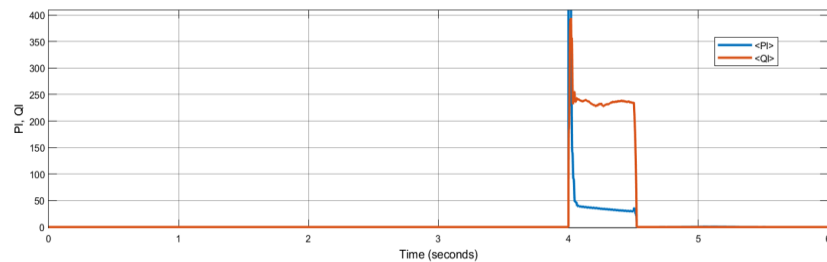


Figure 4.66: Active and Reactive Components of Induction Motor Load vs Time

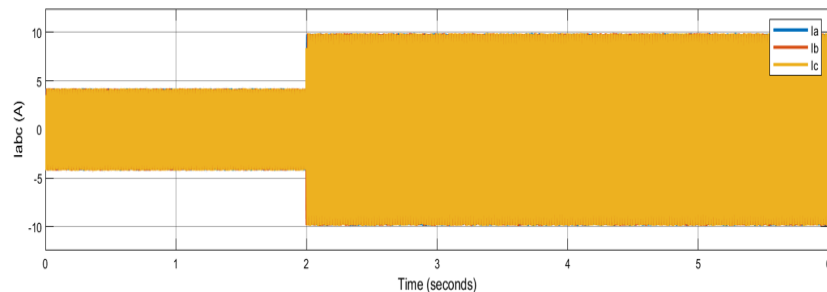


Figure 4.67: Output abc Currents vs Time (PI)

Inference:

This case is similar to case 6 in section 4.1. At $t = 2$ sec, the grid frequency decreases from 50 to 49 Hz. Coupled with that the grid voltage magnitude also drops from 50 to 22.5 V. From $t = 4$ sec to 4.5 sec an induction motor load is injected as well. ANN based controller also performs current and power limiting properties as evident from waveforms. When waveforms of ANN based controller and PI based controller is compared head to head, we can observe

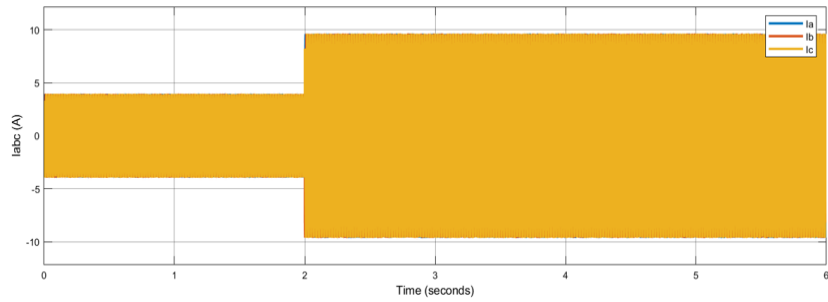


Figure 4.68: Output abc Currents vs Time (ANN)

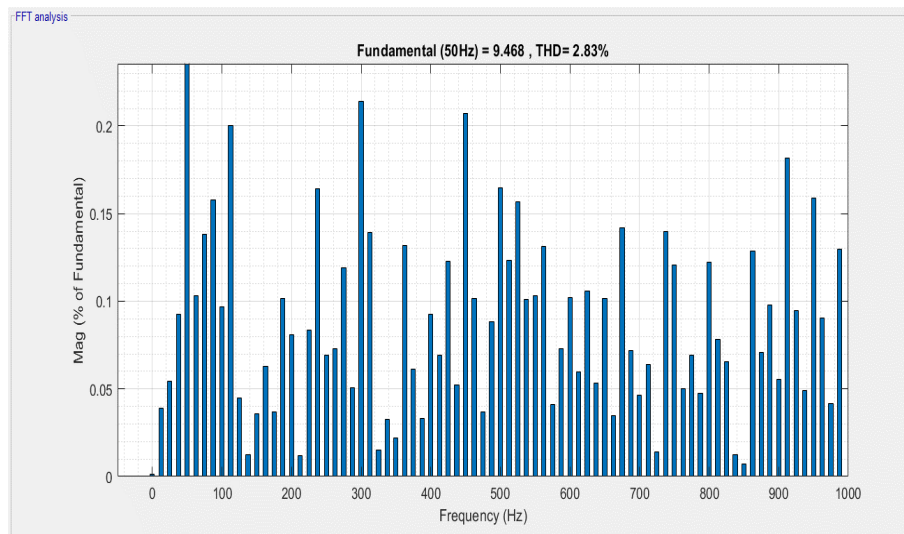


Figure 4.69: PI Based GCDCDG

that noise levels in i_{od} , i_{oq} . Active and Reactive power is significantly less in ANN based GCDCDG as we can clearly observe from the figures waveforms. THD (of output abc currents), Rise time (of i_{od}) and fall time (of i_{oq}) have also improved in ANN based GCDCDG when compared to PI based. Tabular illustration of the inference is given below.

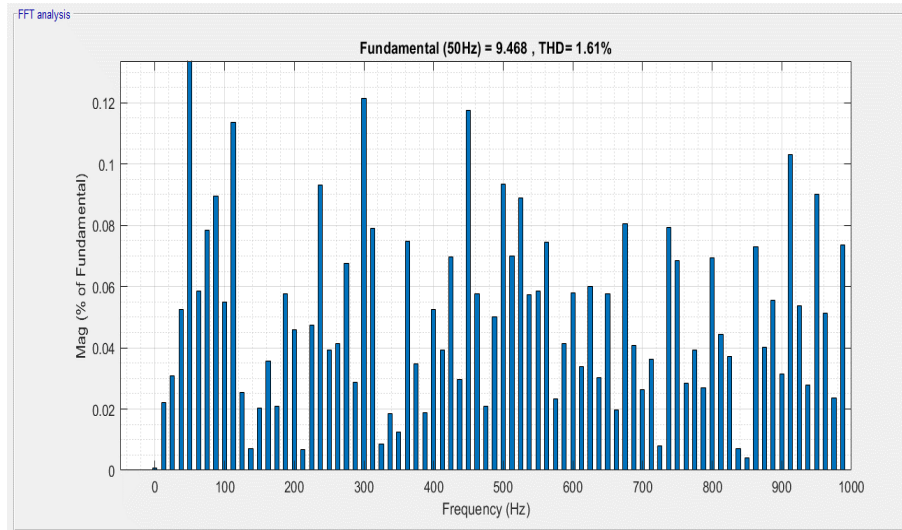


Figure 4.70: ANN Based GCDCDG

PARAMETERS	PI BASED	ANN BASED
THD % OF GRID CURRENT @ $t = 3$ sec	2.83 %	1.61 %
RISE TIME (I_{od})	46.872 ms	38.131 ms
FALL TIME (I_{oq})	43.995 ms	34.157 ms

4.3 Implementation and Comparison With MPC Based Controller

In this third section a Model Predictive Controller(MPC) based GCDCDG controller is implemented. Parameters and initial conditions specified earlier are used here as well. This section has three different case studies, which are similar to earlier sections. Characteristics of ANN and PI based controllers compared with MPC results. Fig 4.71 shows the simulation diagram of a GCDCDG with MPC.

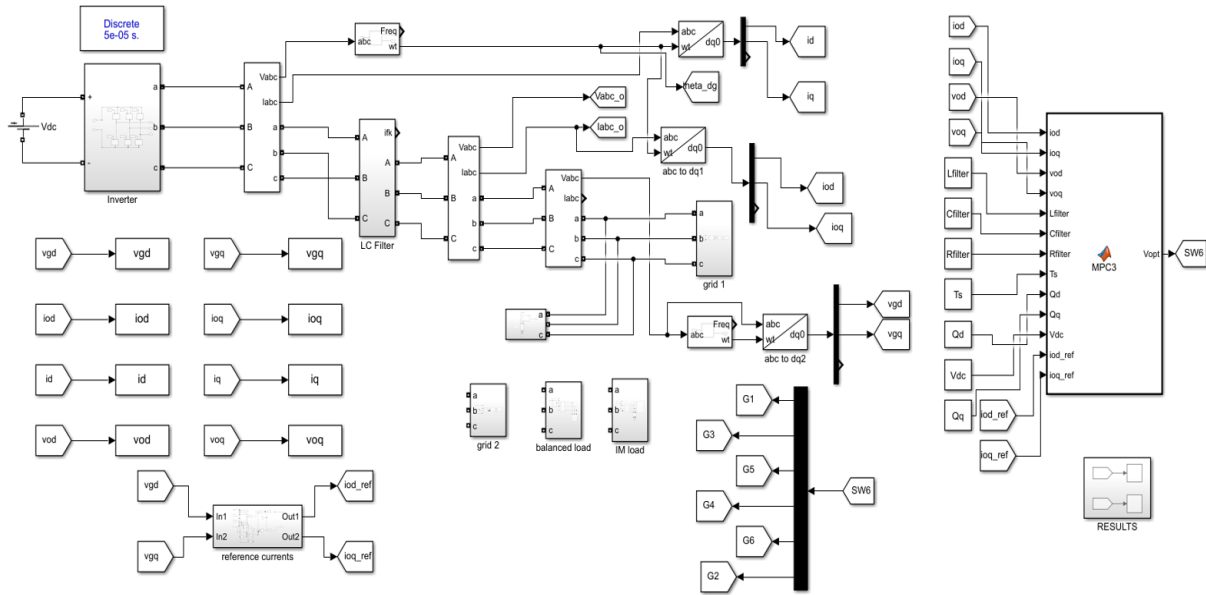


Figure 4.71: MPC Block diagram

4.3.1 Case 1: UG Frequency Drop

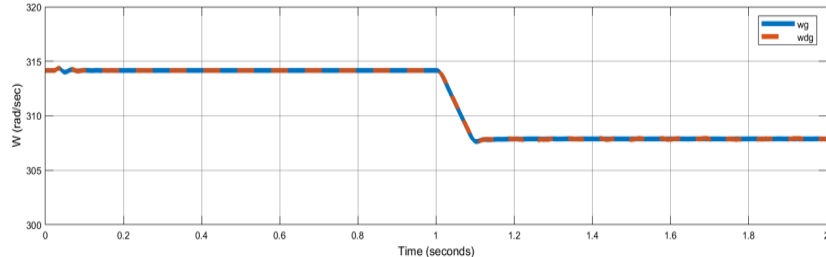


Figure 4.72: DG, Grid Frequency vs Time

In this case UG frequency drops from 50 to 49 Hz at $t = 1$ sec, similar to the cases in the previous sections. MPC based controller also performs current limiting action as evident from the waveforms. Tabular comparison of THD (of output abc current) of all three controllers at this specific case is given below.

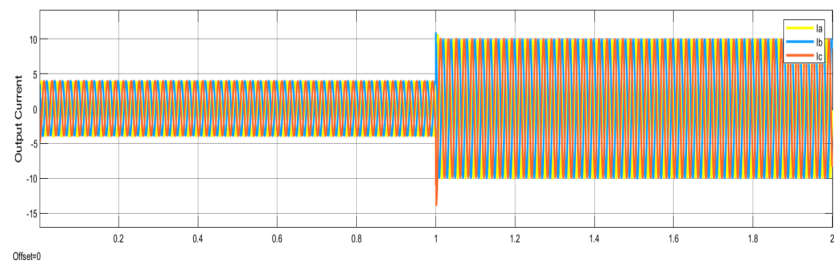


Figure 4.73: Output abc Currents vs Time

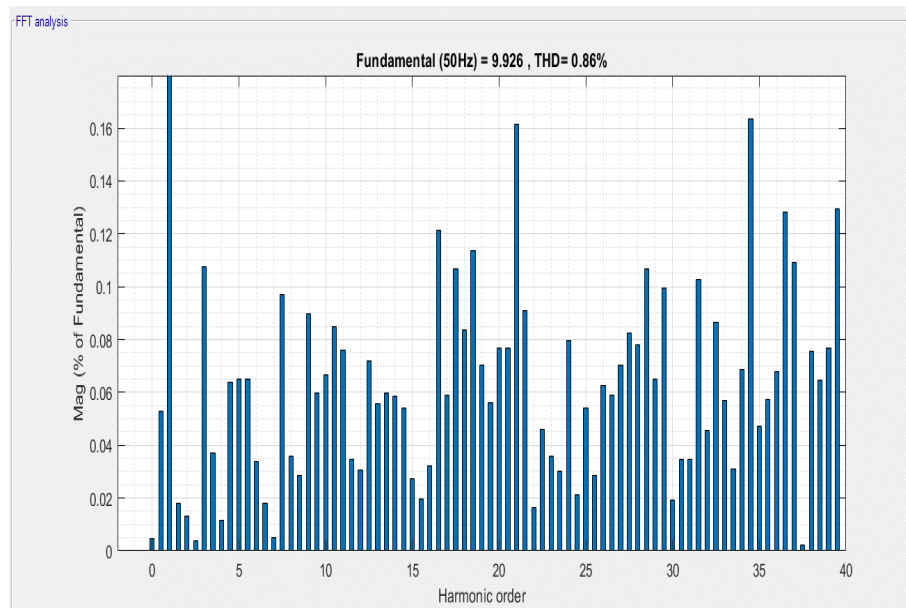


Figure 4.74: Output Current THD at Steady State with MPC Controller

CONFIGURATION	THD OF OUTPUT CURRENT AT STEADY STATE
PI BASED	4.01%
ANN (PI) BASED	2.01%
MPC BASED	0.86%

4.3.2 Case 2: UG Voltage Magnitude Drop

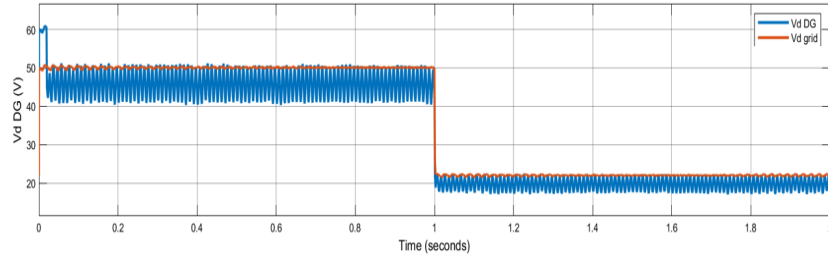


Figure 4.75: DG, Grid Voltage vs Time

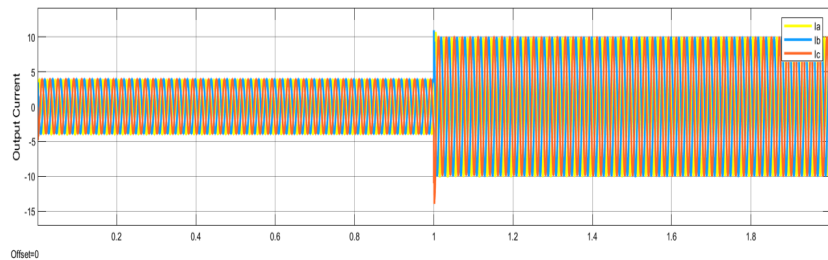


Figure 4.76: Output abc Currents vs Time

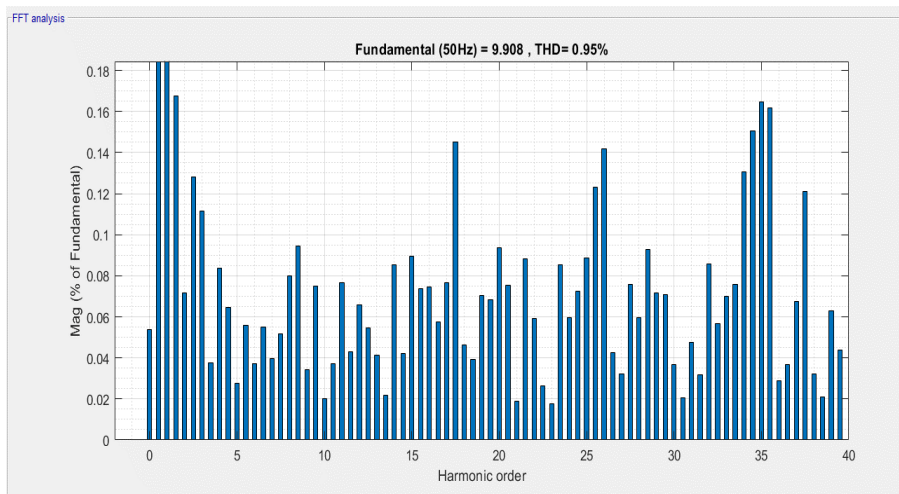


Figure 4.77: Output Current THD at Steady State with MPC Controller

In this case grid voltage magnitude drops from 50 to 22.5 V similar to the cases in the previous sections. MPC based controller also performs current limiting

action as evident from the waveforms. Tabular comparison of THD (of output abc current) of all three controllers at this specific case is given below.

CONFIGURATION	THD OF OUTPUT CURRENT AT STEADY STATE
PI BASED	3.91%
ANN (PI) BASED	1.81%
MPC BASED	0.95%

4.3.3 Case 3: UG Frequency And Voltage Magnitude Drop With Balanced Load Injection

Figure 4.78: DG, Grid Frequency vs Time

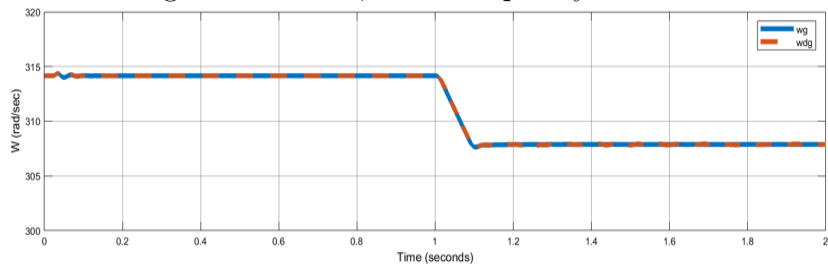


Figure 4.79: DG, Grid Voltage vs Time

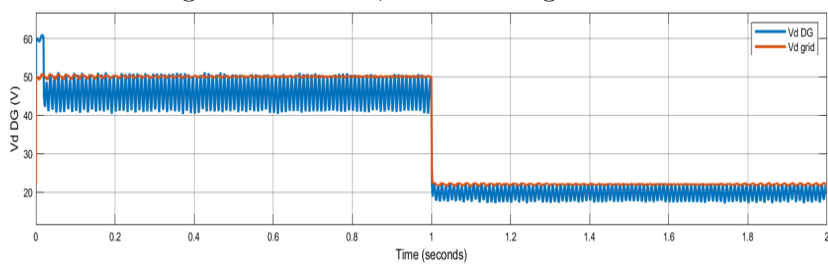


Figure 4.80: Output abc Currents vs Time

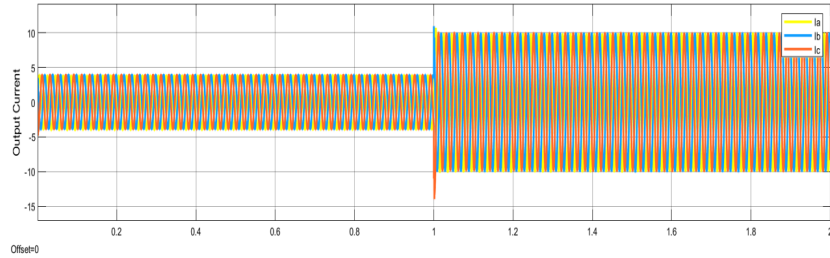


Figure 4.81: Active and Reactive Components of Balanced Load vs Time

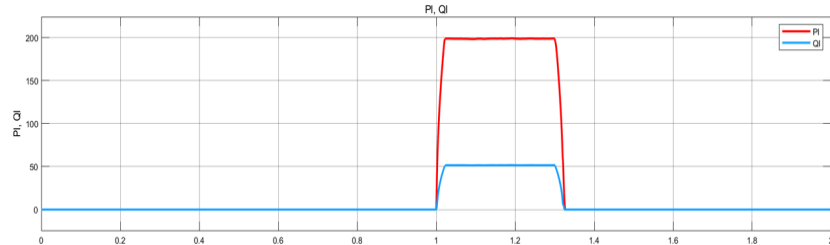
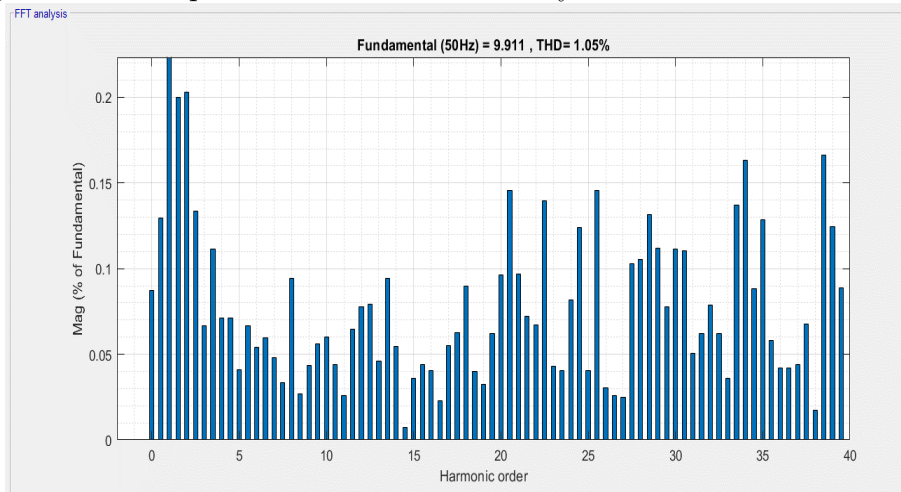


Figure 4.82: Output Current THD at Steady State with MPC Controller



In this case grid voltage magnitude drops from 50 to 22.5 V. Coupled with that the grid frequency also drops from 50 to 49 Hz. Between $t = 1$ sec and $t = 1.3$ sec, a three phase balanced load ($P_L = 174W$ and $Q_L = 45VAr$) is also connected at PCC. similar to the cases in the previous sections. MPC based controller also performs current limiting action as evident from the waveforms. Tabular comparison of THD (of output abc current) of all three controllers at

this specific case is given below.

CONFIGURATION	THD OF OUTPUT CURRENT AT STEADY STATE
PI BASED	3.01%
ANN (PI) BASED	1.60%
MPC BASED	1.05%

From all three cases we can conclude that system with MPC offers superior performance (in terms of THD) while ANN based controller can compete with MPC while having significantly less complexity and computational time.

5 Conclusion

This project work can be essentially split into three parts. The first part of this project work proposes a droop control based current and power limiting strategy for a GCDCDG. This proposed droop-control method limits the output power and currents of GCDCDG under UG frequency reduction, UG voltage magnitude reduction, Balanced load injection, Induction motor load injection and in combination of these scenarios.

The second part of this project work modifies the internal controller of the GCD-CDG by replacing PI controllers on the voltage loop with ANN controllers. The proposed ANN based internal controller limits the output power and current of GCDCDG under the aforementioned case scenarios. The proposed system also improves characteristics like THD of output current and rise time, while also reducing the noise content in output parameters.

In the third part of this project a MPC based controller is developed for the same GCDCDG. MPC based controller was designed to observe how the performance parameters of ANN based internal controller would stack up against a high level controller. From comparison we can conclude that ANN based controller has slightly lesser performance than MPC based controller but at a significantly less computational cost and complexity.

The performance of the proposed methods have been demonstrated by simulation results using MATLAB/Simulink environment under different case studies for an individual GCDCDG.

5.1 Future Scope

This project work can be further expanded by creating a new controller. MPC based controller could be used as the supervisory controller for the ANN based controller. A MPC based ANN controller could potentially have better performance parameters than PI based ANN controller.

Bibliography

- [1] Z. Zhang, C. Dou, D. Yue, B. Zhang, S. Xu, T. Hayat, and A. Alsaedi, “An event-triggered secondary control strategy with network delay in islanded microgrids,” *IEEE Syst. J.*, vol. 13, no. 2, pp. 1851–1860, Jun. 2019.
- [2] M. E. Meral and D. Çelik, “A comprehensive survey on control strategies of distributed generation power systems under normal and abnormal conditions,” *Annu. Rev. Control*, vol. 47, pp. 112–132, Jan. 2019.
- [3] Y. Gupta, S. Doolla, K. Chatterjee, and B. C. Pal, “Optimal DG allocation and Volt–Var dispatch for a droop-based microgrid,” *IEEE Trans. Smart Grid*, vol. 12, no. 1, pp. 169–181, Jan. 2021.
- [4] N. M. Dehkordi and S. Z. Moussavi, “Distributed resilient adaptive control of islanded microgrids under sensor/actuator faults,” *IEEE Trans. Smart Grid*, vol. 11, no. 3, pp. 2699–2708, May 2020.
- [5] Q. Zhong and G. C. Konstantopoulos, “Current-limiting droop control of grid-connected inverters,” *IEEE Trans. Ind. Electron.*, vol. 64, no. 7, pp. 5963–5974, Oct. 2017.
- [6] M. Eskandari and A. V. Savkin, ”On the impact of fault ride-through on transient stability of autonomous microgrids: Nonlinear analysis and solution”, *IEEE Trans. Smart Grid*, vol. 12, no. 2, pp. 9991010, Mar. 2021.
- [7] Y. Peng, Z. Shuai, X. Liu, Z. Li, J. M. Guerrero, and Z. J. Shen, ”Modeling and stability analysis of inverter-based microgrid under harmonic conditions”, *IEEE Trans. Smart Grid*, vol. 11, no. 2, pp. 13301342, Mar. 2020.

-
- [8] M. Ganjian-Aboukheili, M. Shahabi, Q. Sha ee, and J. M. Guerrero, "Seamless transition of microgrids operation from grid-connected to islanded mode", *IEEE Trans. Smart Grid*, vol. 11, no. 3, pp. 21062114, May 2020.
 - [9] Y. Geng, L. Zhu, X. Song, K. Wang, and X. Li, "A modified droop control for grid-connected inverters with improved stability in the fluctuation of grid frequency and voltage magnitude", *IEEE Access*, vol. 7, pp. 7565875669, 2019.
 - [10] H.Yazdanpanahi, Y. W.Li, and W.Xu, "A new control strategy to mitigate the impact of inverter-based DGs on protection system", *IEEE Trans. Smart Grid*, vol. 3, no. 3, pp. 14271436, Sep. 2012.
 - [11] D. M. Vilathgamuwa, P. C. Loh, and Y. Li, "Protection of microgrids during utility voltage sags," *IEEE Trans. Ind. Electron.*, vol. 53, no. 5, pp. 1427–1436, Oct. 2006.
 - [12] D. Çelik and M. E. Meral, "A flexible control strategy with overcurrent limitation in distributed generation systems," *Int. J. Electr. Power Energy Syst.*, vol. 104, pp. 456–471, Jan. 2019.
 - [13] S. Dedeoglu, G. C. Konstantopoulos, and A. G. Paspatis, "Grid-supporting three-phase inverters with inherent root mean square current limitation under balanced grid voltage sags," *IEEE Trans. Ind. Electron.*, vol. 68, no. 11, pp. 11379–11389, Nov. 2021.
 - [14] H. J. Laaksonen, "Protection principles for future microgrids," *IEEE Trans. Power Electron.*, vol. 25, no. 12, pp. 2910–2918, Dec. 2010.
 - [15] X. Guo, W. Liu, X. Zhang, X. Sun, Z. Lu, and J. M. Guerrero, "Flexible control strategy for grid-connected inverter under unbalanced grid faults without PLL," *IEEE Trans. Power Electron.*, vol. 30, no. 4, pp. 1773–1778, Apr. 2015.
 - [16] Z. Chen, X. Pei, M. Yang, L. Peng, and P. Shi, "A novel protection scheme for inverter-interfaced microgrid (IIM) operated in islanded mode," *IEEE Trans. Power Electron.*, vol. 33, no. 9, pp. 7684–7697, Sep. 2018.
 - [17] I. Sadeghkhani, M. E. H. Golshan, J. M. Guerrero, and A. Mehrizi-Sani, "A current limiting strategy to improve fault ride-through of inverter interfaced autonomous microgrids," *IEEE Trans. Smart Grid*, vol. 8, no. 5, pp. 2138–2148, Sep. 2017.
 - [18] L. Zhou, A. Swain, and A. Ukil, "Reinforcement learning controllers for enhancement of low voltage ride through capability in hybrid power systems," *IEEE Trans. Ind. Informat.*, vol. 16, no. 8, pp. 5023–5031, Aug. 2020.

-
- [19] Y. Jiang, X. Li, C. Qin, X. Xing, and Z. Chen, "Improved particle swarm optimization based selective harmonic elimination and neutral point balance control for three-level inverter in low-voltage ride-through operation," *IEEE Trans. Ind. Informat.*, vol. 18, no. 1, pp. 642–652, Jan. 2022.
 - [20] J. Rocabert, A. Luna, F. Blaabjerg, and P. Rodríguez, "Control of power converters in AC microgrids", *IEEE Trans. Power Electron.*, vol. 27, no. 11, pp. 47344749, Nov. 2012.
 - [21] M. E. Meral and D. Çelik, "Proportional complex integral based control of distributed energy converters connected to unbalanced grid system", *Control Eng. Pract.*, vol. 103, pp. 113, Oct. 2020
 - [22] A. Saleh, A. Rastegarnia, A. Farzamnia and K. T. T. Kin, "Power and Current Limiting Strategy Based on Droop Controller With Floating Characteristic for Grid-Connected Distributed Generations," in *IEEE Access*, vol. 10, pp. 13966-13973, 2022.
 - [23] S. Zhao, F. Blaabjerg, and H. Wang, "An overview of artificial intelligence applications for power electronics," *IEEE Trans. Power Electron.*, vol. 36, no. 4, pp. 4633–4658, Apr. 2021.
 - [24] M. Amin and M. Molinas, "Small-signal stability assessment of power electronics based power systems: A discussion of impedance- and eigenvalue-based methods," *IEEE Trans. Ind. Appl.*, vol. 53, no. 5, pp. 5014–5030, Sep. 2017.
 - [25] L. Tarisciotti, P. Zanchetta, A. Watson, J. C. Clare, M. Degano, and S. Bifaretti, "Modulated model predictive control for a three-phase active rectifier," *IEEE Trans. Ind. Appl.*, vol. 51, no. 2, pp. 1610–1620, Mar. 2015.
 - [26] P. R. Bana and M. Amin, "Control for grid-connected VSC with improved damping based on physics-informed neural network," *IEEE J. Emerg. Sel. Topics Ind. Electron.*, vol. 4, no. 3, pp. 878–888, Jul. 2023.
 - [27] F. Toso, A. Favato, R. Torchio, P. Alotto, and S. Bolognani, "Continuous control set model predictive current control of a microgrid-connected PWM inverter," *IEEE Trans. Power Syst.*, vol. 36, no. 1, pp. 415–425, Jan. 2021.
 - [28] A. A. Ahmed, B. K. Koh, and Y. I. Lee, "A comparison of finite control set and continuous control set model predictive control schemes for speed control of induction motors," *IEEE Trans. Ind. Informat.*, vol. 14, no. 4, pp. 1334–1346, Apr. 2018.

-
- [29] I. S. Mohamed, S. Rovetta, T. D. Do, T. Dragicevic, and A. A. Z. Diab, "A neural-network-based model predictive control of three-phase inverter with an output LC filter," *IEEE Access*, vol. 7, pp. 124737–124749, 2019.
 - [30] O. H. Abu-Rub, A. Y. Fard, M. F. Umar, M. Hosseinzadehtaher, and M. B. Shadmands, "Towards intelligent power electronics-dominated grid via machine learning techniques," *IEEE Power Electron. Mag.*, vol. 8, no. 1, pp. 28–38, Mar. 2021.
 - [31] S. Ramachandran, "Applying AI in power electronics for renewable energy systems [expert view]," *IEEE Power Electron. Mag.*, vol. 7, no. 3, pp. 66–67, Sep. 2020.
 - [32] P. R. Bana and M. Amin, "Adaptive vector control of grid-tied VSC using multilayer perceptron-recurrent neural network," in Proc. 47th IEEE IECON, Jul. 2021, pp. 1–6.
 - [33] T. Dragicevic and M. Novak, "Weighting factor design in model predictive control of power electronic converters: An artificial neural network approach," *IEEE Trans. Ind. Electron.*, vol. 66, no. 11, pp. 8870–8880, Nov. 2019.
 - [34] M. Babaie, M. Mehrasa, M. Sharifzadeh, and K. Al-Haddad, "Floating weighting factors ANN-MPC based on Lyapunov stability for seven level modified PUC active rectifier," *IEEE Trans. Ind. Electron.*, vol. 69, no. 1, pp. 387–398, Jan. 2022.
 - [35] M. Babaie, M. Sharifzadeh, M. Mehrasa, and K. Al-Haddad, "Lyapunov based neural network estimator designed for grid-tied nine-level packed E-cell inverter," in Proc. IEEE Appl. Power Electron. Conf. Exposit. (APEC), Mar. 2020, pp. 3311–3315.
 - [36] P. Ranjan Bana, M. Amin and M. Molinas, "ANN-Based Surrogate PI and MPC Controllers for Grid-Connected VSC System: Small-Signal Analysis and Comparative Evaluation," in *IEEE Journal of Emerging and Selected Topics in Power Electronics*, vol. 12, no. 1, pp. 566–578, Feb. 2024.